Dendritic, delayed, and stochastic CaMKII activation underlies behavioral time scale plasticity in CA1 synapses

Anant Jain[1], Yoshihisa Nakahata[1], Tetsuya Watabe[1], Polina Rusina[1], Kelly South[1], Kengo Adachi[1], Long Yan[1], Noriko Simorowski[2], Hiro Furukawa[2], Ryohei Yasuda[1]

[1]Max Planck Florida Institute of Neuroscience, 1 Max Plank Way, Jupiter, FL 334058

[2]Cold Spring Harbor Laboratory, 1 Bungtown Rd, Cold Spring Harbor, NY 11724

These authors contributed equally: AJ, YN

Correspondence to RY. Ryohei.Yasuda@mpfi.org

Abstract

Behavioral time scale plasticity (BTSP), is a form of non-Hebbian plasticity induced by integrating pre- and postsynaptic components separated by behavioral time scale (seconds). BTSP in the hippocampal CA1 neurons underlies place cell formation. However, the molecular mechanisms underlying this behavioral time scale (eligibility trace) and synapse specificity are unknown. CaMKII can be activated in a synapse-specific manner and remain active for a few seconds, making it a compelling candidate for the eligibility trace during BTSP. Here, we show that BTSP can be induced in a

single dendritic spine using 2-photon glutamate uncaging paired with postsynaptic current injection temporally separated by behavioral time scale. Using an improved CaMKII sensor, we saw no detectable CaMKII activation during this BTSP induction. Instead, we observed a dendritic, delayed, and stochastic CaMKII activation (DDSC) associated with Ca^{2+} influx and plateau 20-40 s after BTSP induction. DDSC requires both pre-and postsynaptic activity, suggesting that CaMKII can integrate these two signals. Also, optogenetically blocking CaMKII 30 s after the BTSP protocol inhibited synaptic potentiation, indicating that DDSC is an essential mechanism of BTSP. IP3-dependent intracellular Ca^{2+} release facilitates both DDSC and BTSP. Thus, our study suggests that the non-synapse specific CaMKII activation provides an instructive signal with an extensive time window over tens of seconds during BTSP.

Introduction

Synaptic plasticity is the basis of acquiring and storing new information in the brain [1]. Synaptic plasticity can be induced by specific patterns of electrical activity such as high-frequency synaptic stimulation [2,3], spike-timing-dependent plasticity (STDP) [4-6], or synaptic stimulation coupled with various neuromodulators [7,8]. Ca^{2+} influx via the postsynaptic activation of NMDA receptors (NMDARs) and the downstream synapse-specific activation of CaMKII is the central mechanism that leads to an increase in the dendritic spine volume and AMPAR number and conductance, causing synaptic potentiation [9-13]. In the classical Hebbian mechanism, coordinated pre- and postsynaptic activation leads to a relieve of the Mg^{2+} block in NMDAR, allowing Ca^{2+} ions to flow into dendritic spines.

Despite the extensive cellular and molecular understanding of synaptic plasticity, particularly at hippocampal CA3-CA1 synapses, there is limited direct evidence of specific plasticity mechanisms that occur at these synapses during behavioral learning [14]. Computational studies suggest that the Hebbian plasticity rules that applies to the milliseconds require modification to explain simple learning behaviors that occur over seconds to minutes [15]. Recently, a behavioral time scale plasticity (BTSP) paradigm was discovered at CA3-CA1 synapses and was suggested to be involved in CA1 place cell formation [16,17]. In this plasticity, brief postsynaptic depolarization is paired with presynaptic inputs within a "behavioral time scale" or hundreds of milliseconds to seconds to induce synaptic potentiation during place cell induction. Synaptic potentiation can be induced either by forward pairing (presynaptic stimulation followed by depolarization) or converse pairing (depolarization followed by presynaptic

57　stimulation). BTSP can be interpreted as a product of 1) eligibility trace, an input-

58　specific signal that lasts for a few seconds, and 2) instructive signals by postsynaptic

59　depolarization, which induces synaptic potentiation to the eligible synapse. For the

60　converse BTSP (cBTSP), the instructive signal also needs to influence the synapse-

61　specific signal over a few seconds. Studies suggest that the BTSP requires plateau

62　potential and Ca^{2+} spikes in dendrites, perhaps providing instructive signals [17,18].

63　However, the molecular representations of the eligibility trace and the instructive signal

64　are unknown.

65　Using 2-photon fluorescence lifetime imaging (2pFLIM) of fluorescent resonance energy

66　transfer (FRET) sensor, previous studies have shown that Ca^{2+} Calmodulin-dependent

67　kinase II (CaMKII), a kinase critical for long-term synaptic plasticity [11], is activated in a

68　synapse-specific manner during glutamate uncaging-induced structural plasticity of

69　dendritic spines [19,20]. CaMKII remains active for 1-6 seconds after glutamate uncaging

70　due to autophosphorylation at the T286 site [20,21]. This time scale of CaMKII activation

71　(seconds) makes it a potential entity for the eligibility trace.

72　In the current study, we investigated the role of CaMKII in BTSP using whole-cell

73　electrophysiology, glutamate uncaging, and 2pFLIM imaging of an improved CaMKII

74　conformational sensor in hippocampal slices. First, we developed a glutamate uncaging

75　protocol to induce BTSP at individual dendritic spines. Second, to image CaMKII activity

76　with high sensitivity, we improved the sensitivity of a CaMKII sensor by ~2 fold. Using

77　this sensor, we did not find any evidence that CaMKII is activated during the BTSP

78　protocol. Instead, a dendritic, delayed, and stochastic CaMKII activation (DDSC) occurs

79　several tens of seconds after the induction of BTSP. We confirmed the requirement of

80   DDSC by inhibiting CaMKII using optogenetic CaMKII inhibitor paAIP2 [22] at different

81   time points after BTSP induction. Finally, we found that both DDSC and BTSP require

82   IP3-dependent Ca^{2+} release from internal stores. Our experiments demonstrate the

83   critical role of non-synapse-specific CaMKII activation as an instructive signal spanning

84   an extended time scale (tens of seconds) in BTSP. Furthermore, BTSP appears to be

85   induced by integrating two different time scales, one for integrating pre- and

86   postsynaptic inputs over behavioral time scale to induce DDSC (seconds) and the other

87   for integrating input-specific priming signal with DDSC over tens of seconds.

88

89   **Results**

90   **Behavioral time scale plasticity can be induced in single spines at proximal apical**

91   **dendrites**

92   Previous studies have shown that during place cell formation, activity localized at CA1

93   dendrites precedes the somatic cell firing suggesting synapse-specific activation of

94   plasticity [23]. Thus we investigated whether behavioral time scale plasticity (BTSP),

95   which is one of the mechanisms described for place cell formation [17], can be induced in

96   single spines. To do so, we employed a whole-cell patch-clamp electrophysiology on

97   CA1 neurons in organotypic hippocampal slices and measured 2-photon uncaging-

98   evoked excitatory postsynaptic potentials (EPSPs) from 1-2 spines of secondary

99   branches of proximal apical dendrites before and after the induction of BTSP (**Fig. 1a**).

100 To induce BTSP, we delivered a train of 5 uncaging pulses on one spine at 1 Hz

101 intervals, and then after a 750 ms delay from the last pulse (3.25 s from the center of

102 uncaging pulses), gave a 600 pA current injection pulse for 300 ms (**Fig. 1b**). We found

103 that this protocol induced a 93±16% (n=19) potentiation in EPSP amplitude in the

104 stimulated spines (**Fig. 1d, e**), but not in the adjacent spines (13±10%, n=11, **Fig 1d, e**).

105 We also developed a converse BTSP protocol (cBTSP), in which a current injection

106 (600 pA for 300 ms) was delivered 750 ms before 5 uncaging pulses at 1 Hz (**Fig 1c**).

107 This protocol also induced a similar EPSP potentiation (81±25%, n = 15) in EPSP

108 amplitude in stimulated spines but not in adjacent spines (13±10%, n = 12) (**Fig. 1f, g**).

109 Similarly, in acute hippocampal slices, the BTSP protocol also induced potentiation

110 (103±29%, n = 12) in the stimulated spines but not in adjacent spines (18±7%, n = 8)

111 (**Fig. 1h-j**). These results demonstrate that BTSP can be induced in single dendritic

112 spines in a synapse-specific manner both in acute and organotypic slices.

113 Since basal and distal dendrites receive inputs different from proximal apical dendrites

114 [24], we investigated whether BTSP can also be induced in these dendrites. Notably, the

115 same BTSP protocol failed to induce EPSP potentiation at basal or distal apical

116 dendrites (<200 μm from the soma) (basal: 7±17% n = 10, distal, 12±12%, n = 8) (**Fig.**

117 **1k, l**, **Extended Fig. 1**). Thus, BTSP induction mechanism may depend on the location

118 of dendritic branches. Next, we examined the molecular mechanism of BTSP using

119 pharmacological inhibitors and transgenic mice. We found that voltage-gated sodium

120 channel inhibitor TTX (1 μM) and NMDAR inhibitor APV (50 μM) inhibit BTSP induction

121 in stimulated spines (**Fig. 1k, l, Extended Fig. 1**). Furthermore, mutant mice in which

122 CaMKII activity is reduced (αCaMKII^{T286A}) [25] showed no BTSP (**Fig. 1k, l, Extended**

123 **Fig. 1**). These results suggest that, similarly to the Hebbian LTP, postsynaptic spiking

124 and the activation of NMDAR and CaMKII are required for BTSP induction.

125

Improved CaMKII sensor detected delayed global CaMKII activity after BTSP

induction.

If CaMKII represents the eligibility trace, its activation should be localized in the

stimulated spines and last for a few seconds. This synaptic input will not release the

Mg^{2+} block; thus, Ca^{2+} signaling is likely to be small. To detect anticipated small CaMKII

activity during BTSP, we optimized our CaMKII sensor by putting two accepters in the

original Green Camuiα sensor (2dV-Camui)[19] (**Fig. 2a, Supplementary Note**). We

found that 2dV-Camui displays a 2-fold higher signal with a similar time course

compared to the previous version when tested in cell lines (**Fig. 2b-d, Extended Fig. 2-**

1), and uncaging-evoked CaMKII activation in dendritic spines (note that structural LTP

experiments in Fig. 2 are under zero extracellular Mg^{2+} condition. All other experiments

are performed with 1 mM Mg^{2+}) (**Fig. 2e-g**) [19]. As expected, we observed a fast decay in

CaMKII activation for a sensor in which the critical autophosphorylation site (T286) is

mutated [21] (**Fig. 2h, i**). Also, mutations that turn off calmodulin binding (T305 and T306)

eliminated its activation (**Fig. 2h, Extended Fig. 2-2**). Moreover, we confirmed that this

sensor forms the usual dodecameric holoenzyme based on fluctuation correlation

spectroscopy (FCS) and fluorescence-coupled size-exclusion chromatography (FSEC)

(**Extended Fig. 2-3, 2-4**).

To investigate the CaMKII activity during BTSP, we performed a whole-cell patch-clamp

electrophysiology on 2dV-Camuiα expressing CA1 neurons in organotypic slice culture

and imaged CaMKII activity during BTSP induction (**Fig. 3a**). While there was no

CaMKII activity during BTSP induction (**Fig. 3b-d**), we observed CaMKII activation both

148   in stimulated spines and adjacent shafts with a delay of tens of seconds (**Fig. 3b, c**).

149   This delayed global CaMKII activity shows stochasticity in its timing. We found 76% of

150   dendrites show delayed CaMKII activation, with peak timings ranging from 0 to 100 s,

151   particularly clustered around 30-40 s (**Fig. 3c-e**, n=81 dendrites). In control neurons

152   without any stimulation, we also observed CaMKII activation, but with a significantly

153   lower frequency (**Fig 3c-e,** no-stim, n=21). Similarly, uncaging pulses without current

154   injection (**Extended Fig. 3-1** uncaging, n=19), and current injection without uncaging

155   (**Extended Fig. 3-1**, depolarization, n=16) show CaMKII activation with a frequency

156   substantially lower than in BTSP-induced dendrites. In a subset of experiments where

157   we recorded CaMKII activation before BTSP induction for a longer time (100 s) as well

158   as after BTSP, and we also observed a significant increase in CaMKII activation after

159   BTSP induction (**Extended Fig. 3-1**). The average time course (**Fig. 3f**) showed a

160   downward drift in the measurement, perhaps due to photo-bleaching. However, on top

161   of the drift, there exists a substantial elevation of CaMKII activity in BTSP-induced

162   dendrites ~30-40 secs after BTSP protocol, but not in the control groups. The area

163   under the curve in BTSP-dendrites from 30-40 seconds showed significantly higher

164   CaMKII activation compared with the three controls (**Fig. 3g**, two-way ANOVA with

165   Tukey's correction). We found no difference in the peak amplitude of CaMKII activity

166   between BTSP-induced and control conditions (**Extended Fig. 3-1**), indicating that

167   BTSP increases the frequency, but not the amplitude, of CaMKII activation.

168   In a subset of the above experiments, we recorded EPSP in stimulated spines and

169   found similar BTSP potentiation in the CaMKII labeled neurons (**Extended Fig. 3-2a**).

170   Moreover, there is an inverse correlation between the magnitude of potentiation and the

171 time of CaMKII occurrence after BTSP induction (**Extended Fig. 3-2b**), suggesting that

172 earlier CaMKII activity tends to result in a higher magnitude of potentiation. We also

173 performed CaMKII imaging experiments during the cBTSP protocol (**Extended Fig. 3-**

174 **3**). Similar to forward BTSP, we did not observe any CaMKII during cBTSP protocol but

175 found a delayed stochastic CaMKII activation at 30-60 sec after induction of cBTSP

176 (**Extended Fig. 3-3**). The peak amplitude and the frequency of CaMKII activity were

177 similar between BTSP and cBTSP (**Extended Fig. 3-3**). These experiments suggest

178 that BTSP or cBTSP protocol induces dendritic, delayed, and stochastic CaMKII

179 activation (DDSC). DDSC requires both pre- and postsynaptic components, suggesting

180 that CaMKII upstream signaling can integrate these components.

181 To investigate the spatial profile of DDSC, we imaged CaMKII activity simultaneously in

182 stimulated dendrites and the soma or primary dendrite following BTSP induction (**Fig.**

183 **3h**). We found that DDSC is more predominant in the BTSP-induced dendrites than in

184 the soma or primary dendrites (**Fig. 3i-k**). We found that 50% of the recordings show

185 CaMKII activity specific to the BTSP-stimulated dendrites, while 36% of them show

186 CaMKII activity both in the BTSP dendrite and the soma (or primary dendrite) (**Fig. 3j**).

187 Furthermore, the peak CaMKII amplitude in dendrites was significantly higher in the

188 BTSP-induced dendrites than in the soma or primary dendrites (**Fig. 3k**). We found

189 similar dendrite predominant CaMKII activity in cBTSP protocol as well (n=13,

190 **Extended Fig. 3-4a**), where 48% of the recordings showed dendritic CaMKII only in the

191 stimulated dendrites and showed a significantly larger CaMKII peak amplitude in

192 stimulated dendrites compared to somatic CaMKII (**Extended Fig. 3-4b**). Overall, these

193   experiments suggest that DDSC is compartmentalized to the stimulated dendrite and

194   does not spread throughout the cell.

195   **CaMKII activity is associated with Ca^{2+} and plateau potentials in dendrites.**

196   Since CaMKII activation requires Ca^{2+} elevation [11], we hypothesized that DDSC is

197   associated with dendritic Ca^{2+} elevation. To test this hypothesis, we performed Ca^{2+}

198   imaging by filling the cell with Cal 590 (50-100 μM) dyes in a whole-cell configuration for

199   4 min before and after the BTSP protocol (**Fig. 4a-c**). We confirmed that applying the

200   BTSP protocol to these neurons potentiates EPSPs (**Extended Fig. 4-1**). Consistent

201   with DDSC, we found Ca^{2+} elevations in close correlation with plateau potentials during

202   4 min recordings after application of the BTSP protocol (**Fig. 4b**). The frequency of

203   these delayed Ca^{2+} peaked around 20-30 s, again consistent with DDSC (**Extended**

204   **Fig. 4-2**). Like DDSC, Ca^{2+} elevations also occur before stimulation but are significantly

205   less frequent (**Fig 4c**). The majority of Ca^{2+} events were correlated with plateau

206   potentials (Extended Fig. 4-2)

207   To examine whether these delayed Ca^{2+} transients and the plateau potential

208   correspond to CaMKII activity, we performed simultaneous Ca^{2+} and CaMKII imaging by

209   filling 2dV-Camui transfected CA1 neurons with a Ca^{2+} indicator Cal-590 (50 μM)

210   through patch pipette (**Fig. 4d**). Ca^{2+} elevations during the BTSP protocol, likely due to

211   backpropagating action potentials, were much smaller in amplitude and did not show

212   associated CaMKII events (**Fig. 4e**). However, after BTSP, we observed CaMKII

213   activity, corresponding to DDSC, associated with Ca^{2+} elevation and the plateau

214   potential (**Fig. 4d, Extended Fig. 4-1d**). Ca^{2+} triggered average of CaMKII activity

215   clearly showed that the onset of CaMKII activation is temporally aligned with Ca^{2+}

216   elevation (**Fig. 4e).** Both Ca^{2+} and CaMKII events are much larger during delayed

217   events compared to those during the BTSP protocol (**Fig. 4g, h**).

218   **DDSC is required and sufficient as an instructive signal for BTSP**

219   To test whether DDSC is essential in BTSP induction, we transduced neurons with a

220   photo-inducible CaMKII inhibitor paAIP2 [22] using AAV, and inhibited CaMKII 0 or 30 s

221   after BTSP induction by illuminating with blue light (470 nm, BL) (**Fig 5a, b**). Control

222   CA1 neurons, which express paAIP2 but with no BL exposure, showed potentiation in

223   EPSP after the BTSP protocol (89 ± 20%, n = 12) (**Fig. 5c, d**). However, when we

224   inhibited CaMKII 0 or 30 s after BTSP protocol by BL, significantly less synaptic

225   potentiation was induced (11 ± 14% for BL with 0 s delay, n = 10, 14 ± 8% for 30 s

226   delay, n = 11, **Fig. 5c-g**). These results suggest that DDSC is necessary for BTSP

227   induction.

228   To study whether DDSC is sufficient as an instructive signal in BTSP, we applied BTSP

229   protocol under inhibition of Ca^{2+} spikes by the voltage clamp and bath-applied TTX (1

230   μM) and then artificially induced delayed Ca^{2+}-CaMKII signaling by a long, delayed

231   depolarization (10-12 s delay, 20 s width) [19] (**Fig. 5h**). In control neurons, a protocol

232   similar to BTSP, a train of 5 uncaging pulses at 1 Hz paired with depolarization to 0 mV

233   after a 750 ms delay, failed to induce synaptic potentiation (7 ± 8%, n=10) (Fig. **5i-k**).

234   However, in separate experiments, when the long depolarization pulse was delivered

235   10-12 s after the BTSP protocol, we observed a potentiation of EPSC amplitude in the

236   stimulated spines (56.3 ± 16%, n = 11) (**Fig. 5i-k**), suggesting that the depolarization-

237   induced CaMKII [19] provided instructive signals. Taken together with optogenetic

238   experiments, these experiments demonstrate that depolarization that likely activates

239   global CaMKII provides an instructive signal essential for inducing synapse-specific

240   BTSP.

Intracellular calcium release is required for the induction of BTSP and DDSC

242   A previous study has shown that intracellular Ca^{2+} release from internal stores is

243   required for in vivo BTSP-induced place cell formation [26]. Furthermore, the intracellular

244   store-induced Ca^{2+} release has been shown to be induced by IP3-dependent

245   mechanisms [27]. Thus, we investigated the role of intracellular Ca^{2+} release in BTSP and

246   DDSC using thapsigargin (1 μM), which depletes internal stores, or xestospongin C

247   (XestC, 1 μM), which inhibits IP3R. We found that both thapsigargin and XestC

248   significantly inhibited BTSP-induced synaptic potentiation compared to vehicle (DMSO)

249   (**Fig. 6a, b**). Thus, IP3-dependent intracellular Ca^{2+} release from internal stores is

250   required for BTSP. Moreover, CaMKII imaging showed that DDSC was impaired in the

251   presence of thapsigargin or XestC (**Fig 6c-f**). Both drugs reduced the frequency (**Fig.**

252   **6d, e**) and peak amplitude of DDSC (**Fig. 6f**). Overall, these experiments suggest that

253   Ca^{2+} release from internal stores is required for BTSP and DDSC.

254

Discussion

256   BTSP has been a leading model to explain the induction of CA1 place cells. Our

257   uncaging-evoked behavioral time scale plasticity (BTSP) can be induced in a synapse-

258   specific manner, like Hebbian plasticity [28,29]. This also supports previous studies

259   demonstrating that input-specific dendritic plasticity underlies the place cell formation at

260   a specific location [23,30,31].

261 Although the synapse-specific role of CaMKII in synaptic potentiation has been

262 speculated, we did not observe any detectable CaMKII activation during the BTSP

263 protocol, even with our improved CaMKII sensor. However, we cannot rule out the

264 possibility that there is still some activation of CaMKII below our detection limit during

265 BTSP. Instead, we observed a dendritic, delayed, and stochastic CaMKII activity that

266 spreads to the dendrite and nearby spines (DDSC). DDSC appears restricted to BTSP-

267 induced dendrites and did not spread throughout the cell. Our photo-inhibition and

268 voltage-clamp experiments suggest that DDSC plays an essential role in BTSP

269 induction.

270 It is mechanistically intriguing how the pre and postsynaptic components can get paired

271 over several hundred milliseconds and still result in an NMDAR-dependent and

272 synapse-specific plasticity. Although the time constant of CaMKII activation during

273 Hebbian plasticity matches with the eligibility trace of BTSP, our study suggests that

274 CaMKII is not the eligibility trace, since CaMKII activation during BTSP neither is

275 specific to the stimulated synapse nor active for the behavioral time scale. However, the

276 global and delayed nature of DDSC would be consistent with its role as an instructive

277 signal, although it provides a time window much larger than the proposed instructive

278 signal [32]. Since DDSC requires both pre- and postsynaptic components, additional

279 biochemical signaling must exist upstream of CaMKII signaling (**Fig. 6g**). Furthermore,

280 since BTSP-induced synaptic potentiation is spine-specific, the protocol needs to

281 activate synapse-specific signaling to "prime" the stimulated spine, potentially through

282 the metabotropic function of NMDA receptors [33,34]. Overall, there are at least two time

283 scales in this model, one for integrating pre- and postsynaptic inputs over the behavioral

284   time scale (~1 s), and the other for associating the synapse-specific priming signal and

285   the instructive signal via plateau and DDSC (20-40 s). The integration during the

286   behavioral time scale does not need the synapse specificity, as pre- and post-signal

287   integration can occur in the dendrite, leading to delayed plateau potentials and DDSC

288   (**Fig. 6g**). The signal association during the slow time scale appears to give rise to the

289   synapse specificity of BTSP (**Fig. 6g**).

290   BTSP-induced plateau potentials require voltage-gated Ca^{2+} channels to elevate Ca^{2+}

291   [17]. Since our results indicate that DDSC and BTSP need IP3-dependent Ca^{2+} store

292   release, additional amplification of Ca^{2+} by Ca^{2+}-induced Ca^{2+} release (CICR) may be

293   required for high Ca^{2+} elevation sufficient for DDSC and BTSP (**Fig. 6g**). Alternatively,

294   IP3-induced Ca^{2+} release may be responsible for generating delayed Ca^{2+} plateau, as

295   Ca^{2+} store release can be stochastic and global [27]. The requirement of Ca^{2+} store

296   release is consistent with the fact that our protocol did not induce BTSP in basal

297   dendrites. It has been reported that basal and apical dendrites have different properties

298   of the ER-mitochondrial coupling, which is essential for BTSP during place cell

299   formation [26].

300   A brief current injection during our BTSP protocol did not result in a sustained plateau

301   potential [35]. This suggests that BTSP does not require plateau potential at the moment

302   of the induction protocol. Instead, BTSP can facilitate the later induction of plateau

303   potentials associated with DDSCs. This induction of plateau potentials and DDSCs by

304   BTSP provides an extended time window of tens of seconds for associating temporarily

305   separated events.

306

Acknowledgments

Methods

Animals: All experimental procedures were approved and carried out in accordance with the regulations of the Max Planck Florida Institute for Neuroscience Animal Care and Use Committee as per the guidelines by the US National Institutes of Health. P4-P8 mouse pups from both sexes were used to prepare organotypic slices for imaging studies. We used $Camk2a^{T286A}$ mice to test the requirement of CaMKII in BTSP experiments [25].

Plasmid constructs: We fused two dimVenus (Venus$_{A206K, Y145W}$) and mEGFP (EGFP$_{A206K}$) to rat CaMKIIα subunit (2dV-Camuiα) [19,36]. T286A or T305D/T306D 2dV-Camuiα mutants were constructed by restriction digestion and ligation.

328 **Organotypic hippocampal slice cultures and transfection**: Organotypic hippocampal

329 slices were prepared from wild-type or transgenic postnatal 4-8 day-old mouse pups of

330 both sexes as previously described [37]. In brief, the animal was anesthetized with

331 isoflurane, after which it was quickly decapitated and the brain removed. The

332 hippocampi were dissected and cut into 350 μm thick coronal hippocampal slices using

333 a McIlwain tissue chopper (Ted Pella, Inc) and plated on hydrophilic PTFE membranes

334 (Millicell, Millipore) fed by culture medium containing MEM medium (Life Technologies),

335 20% horse serum, 1 mM L-Glutamine, 1 mM $CaCl_2$, 2 mM $MgSO_4$, 12.9 mM D-Glucose,

336 5.2 mM $NaHCO_3$, 30 mM HEPES, 0.075% Ascorbic Acid, 1 μg/ml insulin. The slices

337 were incubated at 37 °C in 5% CO_2. After 7-12 days in culture, CA1 pyramidal neurons

338 were transfected with biolistic gene transfer using 1.0 μm gold beads (8–12 mg) coated

339 with 2dV-Camuiα (50 μg) [38]. Neurons expressing 2dV-Camuiα were imaged 1–5 days

340 after transfection.

341 **Acute slice preparation**: Male mice (P25–P35) were sedated by isoflurane inhalation

342 and perfused intracardially with a chilled choline chloride solution. The brain was

343 removed and placed in the same choline chloride solution composed of 124 mM

344 Choline Chloride, 2.5 mM KCl, 26 mM $NaHCO_3$, 4 mM $MgCl_2$, 1.2 mM $NaH2PO_4$, 10

345 mM Glucose, and 0.5 mM $CaCl_2$, pH 7.4 equilibrated with 95%O_2/5%CO_2. Coronal

346 hippocampal slices (300 μm) from both hemispheres were cut using a vibratome

347 (V1200, Leica) and maintained in a submerged chamber in ACSF at 32°C for 1h and

348 then at room temperature in oxygenated ACSF.

349 **Two-photon glutamate uncaging**: Two-photon glutamate uncaging was performed

350 during BTSP and structural LTP experiments in organotypic hippocampal cultures and

351 acute hippocampal slices as described previously [39]. Experiments were performed in a

352 small recirculating volume (~ 8 ml) of continuously oxygenated ACSF containing 4 mM

353 4-methoxy-7-nitroindolinyl-caged-l-glutamate (MNI-caged glutamate). Ti: Sapphire laser

354 tuned at a wavelength of 720 nm to uncage MNI-caged glutamate in a small region ~0.5

355 µm from the spine. For structural plasticity experiments, 30 uncaging pulse, 0.5 Hz train

356 was given. The power of the laser was set to 2.7 mW measured at the objective. These

357 structural plasticity experiments were performed in Mg^{2+} free artificial cerebral spinal

358 fluid (ACSF; 127 mM NaCl, 2.5 mM KCl, 4 mM $CaCl_2$, 25 mM $NaHCO_3$, 1.25 mM

359 NaH_2PO_4 and 25 mM glucose) containing 1 µM tetrodotoxin (TTX) and 4 mM MNI-

360 caged L-glutamate aerated with 95% O_2 and 5% CO_2. Experiments were performed at

361 room temperature (24–26°C).

362 **Electrophysiology**: Whole cell patch clamp electrophysiology experiments were

363 combined with glutamate uncaging to induce BTSP at individual dendritic spines. The

364 cells were first visualized in a bright field, or for the labelled cells, epifluorescence

365 microscopy. The patch pipette (with tip resistance 2-5 MΩ) included the internal

366 solution containing 145 mM K gluconate, 14 mM phosphocreatine, 4 mM NaCl,

367 0.3 mM NaGTP, 4 mM MgATP, 3 mM L-ascorbic acid, 50-100 µM Alexa-594, and

368 10 mM HEPES (pH 7.4, 294 mOsm). In BTSP experiments, the EPSPs were

369 measured under the current-clamp mode by a patch-clamp amplifier (MC-700B,

370 Molecular Devices) and digitizer (National Instruments). After 2-5 mins of dye loading,

371 fluorescence from Alexa-594 was used to find dendritic spines in 2pFLIM. Uncaging-

372 evoked EPSPs were induced on 1-2 spines on a dendrite by MNI glutamate uncaging,

373 ~0.5 µm away from the tip of the spine. The uEPSP amplitude was 0.4-2 mV. Pairing

374 LTP and some BTSP experiments were performed in voltage-clamp configuration,

375 where the cells were held at -70 mV. The baseline glutamate uncaging evoked EPSC

376 amplitude was between 5-20 pA. Some BTSP experiments were performed in voltage

377 clamp with Cs internal solution containing 130 mM Cs-methanosulphonate, 6 mM KCl,

378 10 mM HEPES, 4 mM NaCl, 0.3 mM MgGTP, 4 mM MgATP, and 14 mM Tris-

379 phosphocreatine (BTSP voltage clamp protocol). Experiments were performed at room

380 temperature (24-26 ^{o}C). In the CaMKII imaging experiments, similar to the above

381 experiments, Alexa 594 dye (100 µM) was loaded as a structural marker. EPSPs were

382 measured before and after the induction of BTSP. In all whole-cell recordings, the series

383 resistance was monitored to be between 10-40 MΩ throughout the recording.

384 **HeLa cell maintenance, transfection and imaging**: HeLa cells (ATCC CCL-2) were

385 grown in Dulbecco's modified Eagle medium supplemented with 10% fetal bovine serum

386 at 37□°C in 5% CO_2. Plasmids were transfected into HeLa cells using Lipofectamine

387 3000 (Invitrogen). Imaging was performed 24-48 h following transfection in a HEPES-

388 buffered ACSF solution (20 mM HEPES pH 7.3, 130 mM NaCl, 2 mM $NaHCO_3$, 25 mM

389 D-glucose, 2.5 mM KCl, 1.25 mM NaH_2PO_4) with 2 mM $CaCl_2$ and 2 mM $MgCl_2$ by

390 2pFLIM as described below. When indicated, cells were stimulated with bath application

391 of ionomycin (1704, Tocris) and then EGTA.

392 **Fluorescence-coupled size-exclusion chromatography (FSEC)**: Expression vector

393 DNAs (2 µg) including Camuiα were transfected into HEK293S GnTI- cells (2 x 106

394 cells per well in 6-well plates) cultured in FreeStyle 293 (Thermo Fisher), using the

395 TransIT2020 transfection reagent (Mirus Bio). Cells were harvested 48 h post-

396 transfection, washed with ice-cold PBS, and sonicated in 250 µl of the TBS (20 mM

397 Tris-HCl (pH 8.0) and 200 mM NaCl), using Misonix Sonicator 3000 (3 times, 30 s,

398 power level 9.0). The lysate was ultracentrifuged at 70,000 rpm for 10 min (TLA110

399 rotor). The supernatant (20 µl) was loaded onto the Superose-6 size-exclusion

400 chromatography column (10/300 GL; GE Healthcare), pre-equilibrated with TBS, and

401 run at a flow rate of 0.4 ml/min. The eluent from the Superose-6 column was detected

402 by a fluorometer (RF-10AXL, Shimadzu) with the following settings: excitation, 475 nm;

403 emission, 507 nm; time increment, 0.5 s; integration time, 1 s; and recording time, 75

404 min. The FSEC data points were plotted by OriginPro graphic software (OriginLab).

405 **Fluorescence correlation spectroscopy (FCS)**: HEK293FT cells (Thermo Fisher)

406 were transfected with the plasmids using Lipofectamine 3000 (Thermo Fisher) and

407 cultured for 2 days at 37 °C and 5 % CO_2. After washed the plate wells once in PBS

408 buffer, the cells were lysed for 5 min with M-PER mammalian protein extraction reagent

409 (Thermo Scientific) including Halt protease inhibitor (Thermo Scientific) and 5 mM EDTA.

410 The lysates were centrifuged at 20000g for 10 min and the supernatants were used for

411 the FCS measurement by diluted 2 to 15-fold in PBS buffer including the protease

412 inhibitor. The FCS measurements were performed at 23 °C under 2-photon microscope

413 without laser scanning, equipped with Ti:Sapphire laser (Chameleon Ultra II, Coherent)

414 tuned to a wavelength of 920 nm. The time-correlated single-photon counting (TCSPC)

415 data were collected for 60-120 s using a water immersion objective (LUMPlanFL N 60×

416 NA 1.0 W, Olympus) directly immersed in 300 µL of the lysate solution, a single-photon

417 counting board (Time Harp 260, PicoQuant), and a software of TTTR mode real-time

418 correlator in TimeHarp 260 v3.0. The data analysis was performed with FoCuS-point

419 software [40].

420 **Optical CaMKII inhibition experiments**: The CaMKII inhibition experiments were

421 performed in organotypic hippocampal slices using previously described paAIP2 [22]. In

422 these experiments, slices were virally infected with 0.5-1 µl AAV mixture per slice

423 (containing AAV9-Camk2a-Cre at 2×10^{12} vg/ml (1:1000 dilution, Addgene and rAAV8-

424 DIO-CBA-pAAIP2-mEGP at 4.2×10^{12} vg/ml, UNC GTC Vector Corp) at DIV 4-6 and

425 imaged or patched at DIV 10-13. Cells with robust EGFP expression were used for

426 experiments. Labelled cells were patched with K glu internal and Alexa 594 dye in the

427 patch pipette as described above. 470 nm LED light stimulation (M470L5, Thorlabs)

428 was used to activate paAIP2.

429 **Two-photon microscopy and 2pFLIM**: Custom-built two-photon fluorescence lifetime

430 imaging microscope was used to perform 2pFLIM as previously described [41]. 2pFLIM

431 imaging was performed using a Ti-sapphire laser (Coherent, Chameleon) at a

432 wavelength of 920 nm with a power of 1.0-1.4 mW. Fluorescence emission was

433 collected using a water immersion objective (60×, numerical aperture 0.9, Olympus),

434 divided with a dichroic mirror (565 nm), and detected with two separated photoelectron

435 multiplier tubes placed after wavelength filters (Chroma, 510/70-2p for green and

436 620/90-2p for red). Both red and green channels were fit with photoelectron multiplier

437 tubes (PMT) having a low transfer time spread (H7422P40; Hamamatsu) to allow for

438 fluorescence lifetime imaging. Photon counting for fluorescence lifetime imaging was

439 performed using a time-correlated single-photon counting board (Time-harp 260, Pico-

440 Quant) using custom software developed in C#

441 (https://github.com/ryoheiyasuda/FLIMage_public). 2pFLIM images were collected at

442 64x64 pixels at the frame rate of 7.8 Hz. A second Ti-sapphire laser tuned at a

443 wavelength of 720 nm was used to uncage MNI-caged glutamate.

444 **Ca^{2+} imaging**: Ca^{2+} imaging was performed by loading calcium dyes Cal 590 (50 μM,

445 AAT Bioquest) together with a structural marker Alexa 488 (100 μM, Thermo Fisher

446 Scientific). The intensity of Ca^{2+} sensor were collected at 64x64 pixels at the frame rate

447 of 7.8 Hz with 2pFLIM (lifetime information was not used). The Ca^{2+} response was

448 calculated by normalizing the intensity with the intensity Alexa 488. The membrane

449 voltage was also recorded during Ca^{2+} imaging under the current-clamp mode. In a

450 subset of experiments, uncaging-evoked EPSPs were measured before and after BTSP

451 induction. In experiments where simultaneous Ca^{2+} and CaMKII experiments were

452 performed, Ca^{2+} was normalized to the average of first 100 frames before the induction

453 of BTSP. The Ca^{2+} events were detected using a custom python code, where 3 times

454 the standard deviation of the baseline noise was used as a detection threshold after the

455 subtraction of basal trend line obtained by linear regression.

456 **2pFLIM analysis**: 2pFLIM analysis was performed as previously described [42]. To

457 measure the fraction of the donor that was undergoing FRET with the acceptor (binding

458 fraction), we fit a fluorescence lifetime curve summing all pixels over a whole image with

459 a double exponential function convolved with the Gaussian pulse response function:

460 $F(t) = F_0[P_D H(t, t_0, \tau_D, \tau_G) + P_{AD} H(t, t_0, \tau_{AD}, \tau_G)]$

461 where τ_{AD} is the fluorescence lifetime of the donor bound with the acceptor, P_D and P_{AD}

462 are the fraction of free donor and donor undergoing FRET with the acceptor,

463 respectively, and $H(t)$ is a fluorescence lifetime curve with a single exponential function

464 convolved with the Gaussian pulse response function:

465    $H(t, t_0, t_D, t_G) = \frac{1}{2}\exp\left(\frac{\tau_G^2}{2\tau_D^2} - \frac{t-t_0}{\tau_i}\right)\text{erfc}\left(\frac{\tau_G^2 - \tau_D(t-t_0)}{\sqrt{2}\tau_D\tau_G}\right),$

466   in which τ_D is the fluorescence lifetime of the free donor, τ_G is the width of the Gaussian

467   pulse response function, F_0 is the peak fluorescence before convolution and t_0 is the

468   time offset, and erfc is the complementary error function.

469   We fixed τ_D to the fluorescence lifetime obtained from free mEGFP (2.6 ns). For

470   experimental data, we fixed τ_D and τ_{AD} to these values to obtain stable fitting.

471   To generate the fluorescence lifetime image, we calculated the mean photon arrival

472   time, $<t>$, in each pixel as:

473    $<t> = \int tF(t)\,dt / \int F(t)\,dt,$

474   Then, the mean photon arrival time is related to the mean fluorescence lifetime, $<\tau>$, by

475   an offset arrival time, t_o, which is obtained by fitting the whole image:

476    $<\tau> = <t> - t_0.$

477   For small regions-of-interest (ROIs) in an image (spines or dendrites), we calculated the

478   binding fraction (P_{AD}) as:

479    $P_{AD} = \tau_D\,(\tau_D - <\tau>)\,(\tau_D - \tau_{AD})^{-1}(\tau_D + \tau_{AD} - <\tau>)^{-1}.$

480   To measure the CaMKII time of occurrence and peak lifetime change in BTSP and

481   control experiments, the raw traces were first normalized using the first 100 frames as

482   baseline and then the normalized data was smoothened using a moving average of 60

483   data points. Following this processing, the time of CaMKII peak and amplitude was

484   manually calculated on individual CaMKII traces.

485   **Experimental design and statistical analysis:** All values are presented as mean ±

486   SEM unless otherwise noted. Number of independent measurements/cells (n) is

487   indicated in figures or figure legends. For our pharmacology experiments, 1-2 control

488 experiments were performed on the same slices before the specific drug was added in

489 the ACSF. In experiments where DMSO was used as a vehicle, we performed control

490 experiments on different days but on the slices made from the same litter as used in the

491 experiments. Unpaired two-tailed student's t test was used for comparing two

492 independent samples. One way ANOVA followed by multiple comparison tests was

493 used for comparing more than two independent samples. Two way ANOVA followed by

494 multiple comparison test was used to compare grouped data sets. Correlation analysis

495 was done by computing Pearson correlation coefficients. Data smoothening, statistical

496 tests and p values are noted in each figure legend and were computed using GraphPad

497 Prism 7.03 for Windows, GraphPad Software, La Jolla California

498 USA, www.graphpad.com.

499

500

Supplementary note: Characterization of new CaMKII sensors

Sensor Screening in HeLa cells

Original Green-Camuiα sensor (1dV-Camui) is made of CaMKIIα subunit fused with dimVenus (Venus$_{A206K, Y145W}$ or dV) and mEGFP (EGFP$_{A206K}$) at N- and C-termini, respectively. To improve the sensor, we screened several modified sensors (**Extended Fig. 2-1**) [19]. We tested Camui with multiple acceptors (2dV-Camui and 3dV-Camui). Also, we tested a variant in which dimVenus is replaced by ShadowY (ShY) [22], which has an even lower quantum yield compared to dimVenus (1ShY-Camui and 2ShY-Camui).

In HeLa cells, we measured fluorescence lifetime changes in response to the bath application of ionomycin (3 μM) using 2pFLIM. Then, the decay kinetics of the sensors was measured by applying EGTA (8 mM). We found that all sensors show qualitatively similar kinetics (**Extended Fig. 2-1b, c**). For dimVenus, we found a larger number of accepters provide a better signal and lower basal fluorescence lifetime, due to high FRET efficiency (**Extended Fig. 2-1d, e**). However, Camui with ShY did not show a clear correlation between the number of accepters and FRET signals (**Extended Fig 2-1d, e**).

While 3dV-Camui provided the best signal among these sensors, we decided not to use this sensor because it did not express well in neurons. Among others, we found that 2dV-Camui showed the best signal-to-background ratio (**Extended Fig. 2-1b,c**), and thus further analyzed this sensor.

522   To validate 2dV-Camui sensor, we analyzed their mutants (**Extended Fig. 2-2**). When

523   we mutated an autophosphorylation site that prolongs CaMKII activation (T286A) [11,21,43-

524   45], the sensor signal was substantially reduced (**Extended Fig. 2-2**). Furthermore, when

525   we eliminated calmodulin binding required for CaMKII activation (T305D and T306D)

526   [46,47], the sensor signal was abolished (**Extended Fig. 2-2**). These results are consistent

527   with previously described CaMKII behavior [11].

528   **Fluctuation correlation analysis**

529   CaMKII holoenzyme consists of dodecamer. Thus, we next studied if they can form

530   dodecamer using fluctuation correlation spectroscopy (FCS) of the lysate of HEK293FT

531   cells expressing CaMKII sensors (**Extended Fig. 2-3**). FCS allows us to measure the

532   diffusion speed of fluorescence molecules by measuring the time correlation of the

533   fluorescence in a focused laser spot. Since the diffusion is sensitive to the

534   hydrodynamic diameter, we can estimate the size of fluorescence particles in the lysate

535   [48]

536   We found that all EGFP-CaMKII, 1dV-Camuiα, 2dV-Camui, 3dV-Camui, 1ShY-Camui,

537   2ShY-Camui showed similar diffusion constant (~10 μm^2/s), suggesting that increasing

538   the number of accepters do not affect the hydrodynamic diameter (**Extended Fig. 2-3a**).

539   In comparison, the diffusion constant of EGFP (84 ± 2.9 μm^2/s) and monomeric

540   CaMKIIα (truncated CaMKIIα[1-306]) (62 ± 2.0 μm^2/s) was much higher consistent with

541   their smaller hydrodynamic diameters [48]

542   The diffusion speed of the sensors is somewhat smaller than previously measured

543   diffusion of non-labeled CaMKII by dynamic light scattering (25 μm^2/s) [49], perhaps

544   because of the fluorophore fusion. To further examine if they can co-polymerize with

545   non-labeled CaMKII, we co-expressed non-labeled CaMKII together with CaMKII

546   sensors with different ratios. We found that, as the ratio of non-labeled CaMKII

547   increases, the diffusion constant becomes higher, suggesting that they can

548   copolymerize (**Extended Fig. 2-3a, b**). Also, the y-intercept, which denotes the diffusion

549   of non-labeled CaMKII, shows the diffusion constant similar to the one previously

550   measured.

551   Thus, overall, these experiments suggest that the fusion of multiple accepters do not

552   affect the hydrodynamic radius of the molecule, suggesting that they can form normal

553   size of holoenzyme. Also, the new CaMKII sensor (2dV-Camui) can copolymerize with

554   non-labeled CaMKIIα.

555

556   **Fluorescence coupled size-exclusion chromatography assay**

557   Next, we performed fluorescence coupled size-exclusion chromatography (FSEC) to

558   measure the approximate size of the holoenzyme. Before testing the new sensors, we

559   examined Green Camuiα, and EGFP-tagged CaMKIIα. As reported before [19,36], Green

560   Camuiα shows similar peak retention time with EGFP-tagged CaMKIIα, suggesting that

561   Green Camuiα is a dodecamer [36] (**Extended Fig. 2-4**). Notably, when we tested Green

562   Camuiβ, which uses CaMKIIβ instead of CaMKIIα, we observed an additional peak

563   corresponding to smaller complex (**Extended Fig. 2-4).** When we ran 2dV-Camui on the

564   column, we found that this sensor showed a single peak time similar to EGFP-CaMKIIα

565 and 1dV-Camuiα. Thus, taken together with FCS analysis, we concluded that 2dV-

566 Camuiα can form dodecamer holoenzyme.

567

568 **Characterization of 2dV-Camui with 2-photon glutamate uncaging**

569 Finally, we tested 2dV-Camui in dendritic spines of pyramidal CA1 neurons in

570 organotypic hippocampal slices. We applied 30 pulses of 2-photon glutamate uncaging

571 in the absence of extracellular Mg^{2+}. Consistent with previous study [21], we found that

572 2dV-Camui is activated in a step-wise manner in response to each uncaging pulse in

573 the stimulated spine, and then decayed with a fast time constant of 7.3 s. The decay

574 time constant was similar to that of 1dV-Camui (7.9 s). These kinetics are consistent

575 with our previous study using the original Green-Camuiα (1dV-Camui) [21]. Furthermore,

576 2dV-Camui with T286A mutation showed much faster decay (0.74 s) (**Fig. 2**), and failed

577 to integrate uncaging pulses (**Fig. 2**), again consistent with our previous work [21]. Finally,

578 we found that the sensor with T305D and T306D mutations abolished the response, as

579 expected [50]. Overall, our results indicate that 2dV-Camui provides signals with the

580 kinetics similar to the original Green-Camuiα, but with ~2 fold higher sensitivity.

581

582

References:

1   Hebb, D. O. *The organization of behavior; a neuropsychological theory*. (Wiley, 1949).

2   Bliss, T. V. & Gardner-Medwin, A. R. Long-lasting potentiation of synaptic transmission in the dentate area of the unanaestetized rabbit following stimulation of the perforant path. *J Physiol* **232**, 357-374 (1973). https://doi.org:10.1113/jphysiol.1973.sp010274

3   Malenka, R. C. & Nicoll, R. A. Long-term potentiation--a decade of progress? *Science* **285**, 1870-1874 (1999). https://doi.org:10.1126/science.285.5435.1870

4   Gerstner, W., Kempter, R., van Hemmen, J. L. & Wagner, H. A neuronal learning rule for sub-millisecond temporal coding. *Nature* **383**, 76-81 (1996). https://doi.org:10.1038/383076a0

5   Markram, H., Lubke, J., Frotscher, M. & Sakmann, B. Regulation of synaptic efficacy by coincidence of postsynaptic APs and EPSPs. *Science* **275**, 213-215 (1997). https://doi.org:10.1126/science.275.5297.213

6   Bi, G. Q. & Poo, M. M. Synaptic modifications in cultured hippocampal neurons: dependence on spike timing, synaptic strength, and postsynaptic cell type. *J Neurosci* **18**, 10464-10472 (1998). https://doi.org:10.1523/JNEUROSCI.18-24-10464.1998

7   Palacios-Filardo, J. & Mellor, J. R. Neuromodulation of hippocampal long-term synaptic plasticity. *Curr Opin Neurobiol* **54**, 37-43 (2019). https://doi.org:10.1016/j.conb.2018.08.009

605 8   Brzosko, Z., Mierau, S. B. & Paulsen, O. Neuromodulation of Spike-Timing-

606   Dependent Plasticity: Past, Present, and Future. *Neuron* **103**, 563-581 (2019).

607   https://doi.org:10.1016/j.neuron.2019.05.041

608 9   Nishiyama, J. & Yasuda, R. Biochemical Computation for Spine Structural

609   Plasticity. *Neuron* **87**, 63-75 (2015). https://doi.org:10.1016/j.neuron.2015.05.043

610 10   Lisman, J., Yasuda, R. & Raghavachari, S. Mechanisms of CaMKII action in

611   long-term potentiation. *Nat Rev Neurosci* **13**, 169-182 (2012).

612   https://doi.org:10.1038/nrn3192

613 11   Yasuda, R., Hayashi, Y. & Hell, J. W. CaMKII: a central molecular organizer of

614   synaptic plasticity, learning and memory. *Nat Rev Neurosci* **23**, 666-682 (2022).

615   https://doi.org:10.1038/s41583-022-00624-2

616 12   Citri, A. & Malenka, R. C. Synaptic plasticity: multiple forms, functions, and

617   mechanisms. *Neuropsychopharmacology* **33**, 18-41 (2008).

618   https://doi.org:10.1038/sj.npp.1301559

619 13   Zha, C. & Sossin, W. S. The molecular diversity of plasticity mechanisms

620   underlying memory: An evolutionary perspective. *J Neurochem* **163**, 444-460

621   (2022). https://doi.org:10.1111/jnc.15717

622 14   Abraham, W. C., Jones, O. D. & Glanzman, D. L. Is plasticity of synapses the

623   mechanism of long-term memory storage? *NPJ Sci Learn* **4**, 9 (2019).

624   https://doi.org:10.1038/s41539-019-0048-y

625 15   Zheng, Y., Liu, X. L., Nishiyama, S., Ranganath, C. & O'Reilly, R. C. Correcting

626   the hebbian mistake: Toward a fully error-driven hippocampus. *PLoS Comput*

627   *Biol* **18**, e1010589 (2022). https://doi.org:10.1371/journal.pcbi.1010589

628   16   Bittner, K. C. *et al.* Conjunctive input processing drives feature selectivity in

629   hippocampal CA1 neurons. *Nat Neurosci* **18**, 1133-1142 (2015).

630   https://doi.org:10.1038/nn.4062

631   17   Bittner, K. C., Milstein, A. D., Grienberger, C., Romani, S. & Magee, J. C.

632   Behavioral time scale synaptic plasticity underlies CA1 place fields. *Science* **357**,

633   1033-1036 (2017). https://doi.org:10.1126/science.aan3846

634   18   Diamantaki, M. *et al.* Manipulating Hippocampal Place Cell Activity by Single-Cell

635   Stimulation in Freely Moving Mice. *Cell Rep* **23**, 32-38 (2018).

636   https://doi.org:10.1016/j.celrep.2018.03.031

637   19   Lee, S. J., Escobedo-Lozoya, Y., Szatmari, E. M. & Yasuda, R. Activation of

638   CaMKII in single dendritic spines during long-term potentiation. *Nature* **458**, 299-

639   304 (2009). https://doi.org:10.1038/nature07842

640   20   Chang, J. Y., Nakahata, Y., Hayano, Y. & Yasuda, R. Mechanisms of

641   Ca(2+)/calmodulin-dependent kinase II activation in single dendritic spines. *Nat*

642   *Commun* **10**, 2784 (2019). https://doi.org:10.1038/s41467-019-10694-z

643   21   Chang, J. Y. *et al.* CaMKII Autophosphorylation Is Necessary for Optimal

644   Integration of Ca(2+) Signals during LTP Induction, but Not Maintenance. *Neuron*

645   **94**, 800-808 e804 (2017). https://doi.org:10.1016/j.neuron.2017.04.041

646   22   Murakoshi, H. *et al.* Kinetics of Endogenous CaMKII Required for Synaptic

647   Plasticity Revealed by Optogenetic Kinase Inhibitor. *Neuron* **94**, 37-47 e35

648   (2017). https://doi.org:10.1016/j.neuron.2017.02.036

649 23   Sheffield, M. E. J., Adoff, M. D. & Dombeck, D. A. Increased Prevalence of

650   Calcium Transients across the Dendritic Arbor during Place Field Formation.

651   *Neuron* **96**, 490-504 e495 (2017). https://doi.org:10.1016/j.neuron.2017.09.029

652 24   Spruston, N. Pyramidal neurons: dendritic structure and synaptic integration. *Nat*

653   *Rev Neurosci* **9**, 206-221 (2008). https://doi.org:10.1038/nrn2286

654 25   Giese, K. P., Fedorov, N. B., Filipkowski, R. K. & Silva, A. J. Autophosphorylation

655   at Thr286 of the alpha calcium-calmodulin kinase II in LTP and learning. *Science*

656   **279**, 870-873 (1998). https://doi.org:10.1126/science.279.5352.870

657 26   O'Hare, J. K. *et al.* Compartment-specific tuning of dendritic feature selectivity by

658   intracellular Ca(2+) release. *Science* **375**, eabm1670 (2022).

659   https://doi.org:10.1126/science.abm1670

660 27   Nakamura, T. *et al.* Inositol 1,4,5-trisphosphate (IP3)-mediated Ca2+ release

661   evoked by metabotropic agonists and backpropagating action potentials in

662   hippocampal CA1 pyramidal neurons. *J Neurosci* **20**, 8365-8376 (2000).

663   https://doi.org:10.1523/JNEUROSCI.20-22-08365.2000

664 28   Matsuzaki, M., Honkura, N., Ellis-Davies, G. C. & Kasai, H. Structural basis of

665   long-term potentiation in single dendritic spines. *Nature* **429**, 761-766 (2004).

666   https://doi.org:10.1038/nature02617

667 29   Harvey, C. D. & Svoboda, K. Locally dynamic synaptic learning rules in pyramidal

668   neuron dendrites. *Nature* **450**, 1195-1200 (2007).

669   https://doi.org:10.1038/nature06416

670 30   Adoff, M. D. *et al.* The functional organization of excitatory synaptic input to place

671   cells. *Nat Commun* **12**, 3558 (2021). https://doi.org:10.1038/s41467-021-23829-y

672   31   Fan, L. Z. *et al.* All-optical physiology resolves a synaptic basis for behavioral

673   timescale plasticity. *Cell* **186**, 543-559 e519 (2023).

674   https://doi.org:10.1016/j.cell.2022.12.035

675   32   Magee, J. C. & Grienberger, C. Synaptic Plasticity Forms and Functions. *Annu*

676   *Rev Neurosci* **43**, 95-117 (2020). https://doi.org:10.1146/annurev-neuro-090919-

677   022842

678   33   Nabavi, S. *et al.* Metabotropic NMDA receptor function is required for NMDA

679   receptor-dependent long-term depression. *Proc Natl Acad Sci U S A* **110**, 4027-

680   4032 (2013). https://doi.org:10.1073/pnas.1219454110

681   34   Stein, I. S., Park, D. K., Claiborne, N. & Zito, K. Non-ionotropic NMDA receptor

682   signaling gates bidirectional structural plasticity of dendritic spines. *Cell Rep* **34**,

683   108664 (2021). https://doi.org:10.1016/j.celrep.2020.108664

684   35   Takahashi, H. & Magee, J. C. Pathway interactions and synaptic plasticity in the

685   dendritic tuft regions of CA1 pyramidal neurons. *Neuron* **62**, 102-111 (2009).

686   https://doi.org:10.1016/j.neuron.2009.03.007

687   36   Takao, K. *et al.* Visualization of synaptic Ca2+ /calmodulin-dependent protein

688   kinase II activity in living neurons. *J Neurosci* **25**, 3107-3112 (2005).

689   https://doi.org:10.1523/JNEUROSCI.0085-05.2005

690   37   Stoppini, L., Buchs, P. A. & Muller, D. A simple method for organotypic cultures

691   of nervous tissue. *J Neurosci Methods* **37**, 173-182 (1991).

692   https://doi.org:10.1016/0165-0270(91)90128-m

693   38   O'Brien, J. A. & Lummis, S. C. Biolistic transfection of neuronal cultures using a

694   hand-held gene gun. *Nat Protoc* **1**, 977-981 (2006).

695   https://doi.org:10.1038/nprot.2006.145

696   39   Colgan, L. A. *et al.* Dual regulation of spine-specific and synapse-to-nucleus

697   signaling by PKCdelta during plasticity. *J Neurosci* (2023).

698   https://doi.org:10.1523/JNEUROSCI.0208-22.2023

699   40   Waithe, D., Clausen, M. P., Sezgin, E. & Eggeling, C. FoCuS-point: software for

700   STED fluorescence correlation and time-gated single photon counting.

701   *Bioinformatics* **32**, 958-960 (2016). https://doi.org:10.1093/bioinformatics/btv687

702   41   Laviv, T. *et al.* In Vivo Imaging of the Coupling between Neuronal and CREB

703   Activity in the Mouse Brain. *Neuron* **105**, 799-812 e795 (2020).

704   https://doi.org:10.1016/j.neuron.2019.11.028

705   42   Yasuda, R. Imaging spatiotemporal dynamics of neuronal signaling using

706   fluorescence resonance energy transfer and fluorescence lifetime imaging

707   microscopy. *Curr Opin Neurobiol* **16**, 551-561 (2006).

708   https://doi.org:10.1016/j.conb.2006.08.012

709   43   Chao, L. H. *et al.* A mechanism for tunable autoinhibition in the structure of a

710   human Ca2+/calmodulin- dependent kinase II holoenzyme. *Cell* **146**, 732-745

711   (2011). https://doi.org:10.1016/j.cell.2011.07.038

712   44   Hanson, P. I., Kapiloff, M. S., Lou, L. L., Rosenfeld, M. G. & Schulman, H.

713   Expression of a multifunctional Ca2+/calmodulin-dependent protein kinase and

714   mutational analysis of its autoregulation. *Neuron* **3**, 59-70 (1989).

715   https://doi.org:10.1016/0896-6273(89)90115-3

716   45   Hanson, P. I., Meyer, T., Stryer, L. & Schulman, H. Dual role of calmodulin in

717   autophosphorylation of multifunctional CaM kinase may underlie decoding of

718   calcium signals. *Neuron* **12**, 943-956 (1994). https://doi.org:10.1016/0896-

719   6273(94)90306-9

720   46   Lou, L. L. & Schulman, H. Distinct autophosphorylation sites sequentially

721   produce autonomy and inhibition of the multifunctional Ca2+/calmodulin-

722   dependent protein kinase. *J Neurosci* **9**, 2020-2032 (1989).

723   https://doi.org:10.1523/JNEUROSCI.09-06-02020.1989

724   47   Jama, A. M., Fenton, J., Robertson, S. D. & Torok, K. Time-dependent

725   autoinactivation of phospho-Thr286-alphaCa2+/calmodulin-dependent protein

726   kinase II. *J Biol Chem* **284**, 28146-28155 (2009).

727   https://doi.org:10.1074/jbc.M109.005900

728   48   Chen, Y., Muller, J. D., Ruan, Q. & Gratton, E. Molecular brightness

729   characterization of EGFP in vivo by fluorescence fluctuation spectroscopy.

730   *Biophys J* **82**, 133-144 (2002). https://doi.org:10.1016/S0006-3495(02)75380-0

731   49   Gaertner, T. R. *et al.* Comparative analyses of the three-dimensional structures

732   and enzymatic properties of alpha, beta, gamma and delta isoforms of Ca2+-

733   calmodulin-dependent protein kinase II. *J Biol Chem* **279**, 12484-12494 (2004).

734   https://doi.org:10.1074/jbc.M313597200

735   50   Pi, H. J., Otmakhov, N., Lemelin, D., De Koninck, P. & Lisman, J. Autonomous

736   CaMKII can promote either long-term potentiation or long-term depression,

737   depending on the state of T305/T306 phosphorylation. *J Neurosci* **30**, 8704-8709

738   (2010). https://doi.org:10.1523/JNEUROSCI.0133-10.2010

739
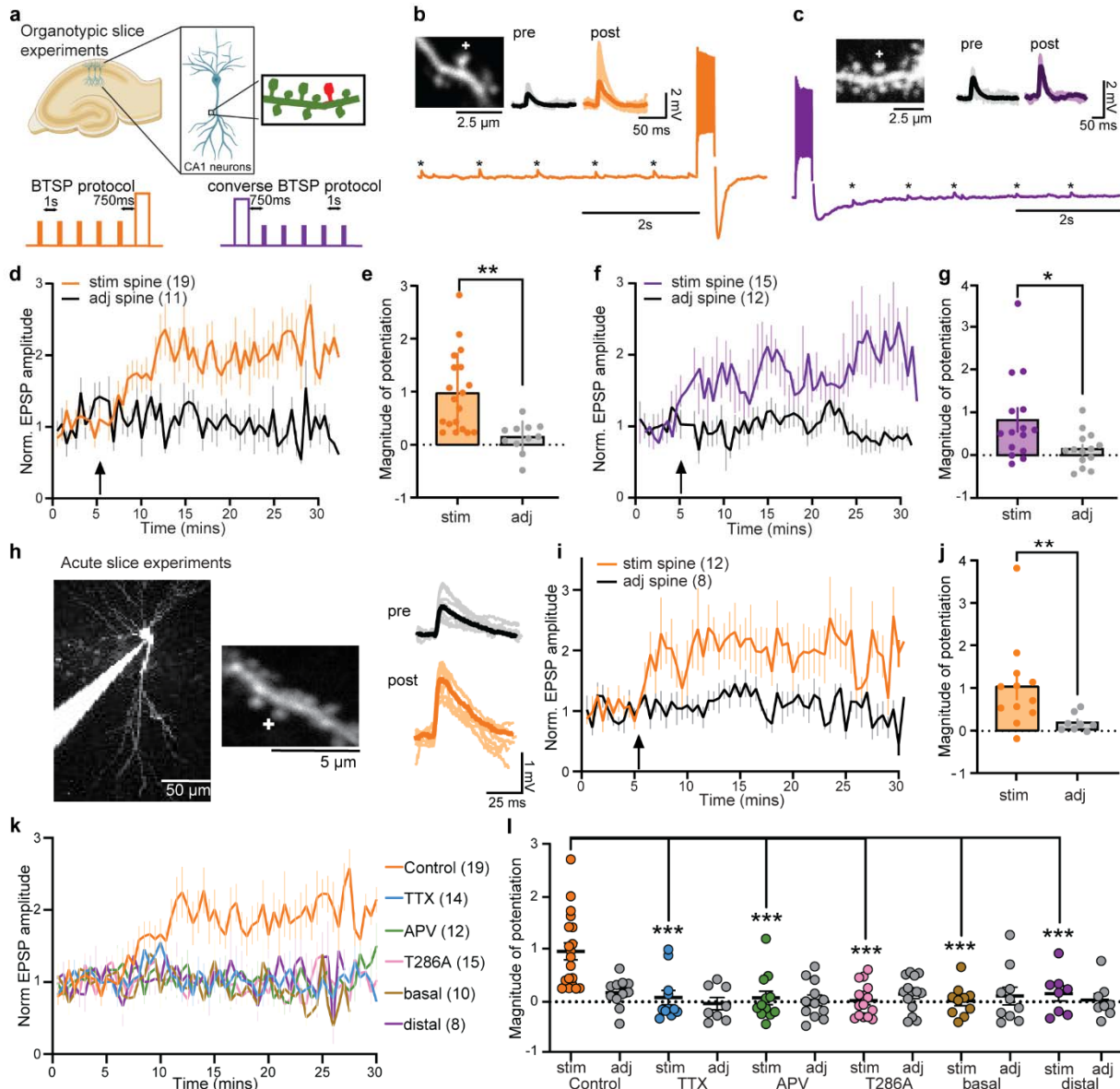
Figure 1: Glutamate uncaging protocols to induce BTSP at proximal apical CA1 dendritic spines.

a, Top: Schematics of the experimental setup. Bottom: BTSP and converse BTSP (cBTSP) protocols: five uncaging pulses were given at an individual spine before (orange) or after (purple) a 600 pA current injection (300 ms) with a delay of 750 ms.

b, A representative image of a dendrite of a CA1 neuron in an organotypic hippocampal slice (right top), uncaging-evoked EPSPs (10 recording and average) before and after

BTSP from the spines on the dendrite (left top), and electrical trace during the BTSP protocol (bottom).

c, Same as b, but with the cBTSP protocol.

d-e, Mean time course (**d**) and summary of the magnitude of potentiation (25-30 min) (**e**) of uncaging-evoked EPSP amplitude normalized to the baseline (0-5 min) at stimulated spines (n=19, orange) and adjacent spines (n=11, black) in response to BTSP protocol (arrow). **p < 0.01, two-tailed t-test.

f-g, Same as c-d, but with cBTSP protocol (n = 15 for stimulated spines and 12 for adjacent spines). *p < 0.05, two-tailed t-test.

h, Left: Representative Alexa 594 filled image of a CA1 neuron and a dendritic shaft in acute hippocampal slices, where BTSP was induced. Right: Uncaging evoked EPSP traces of the stimulated spine before (10 EPSPs) and after (10 EPSPs) induction of BTSP.

i, Averaged time course of normalized EPSP amplitude in response to BTSP induction in stimulated and adjacent spines in acute hippocampal slices. Numbers of cells are in the figure.

j, Summary of the magnitude of potentiation of EPSP amplitude. *p < 0.05, two-tailed t-test, p<0.05.

k-l, Average time course (**k**) and the summary (**i**) of the magnitude of BTSP-induced EPSP potentiation under various conditions. TTX and APV are bath applied. T286A is data from *Camk2a*^{T286A} mice. Basal and distal: BTSP protocol on basal or distal (> 200

µm from the soma) dendrites, respectively. Sample numbers (spines) are in the figure.

Two-way ANOVA with multiple comparison test (Dunnett's correction) ***p<0.001.
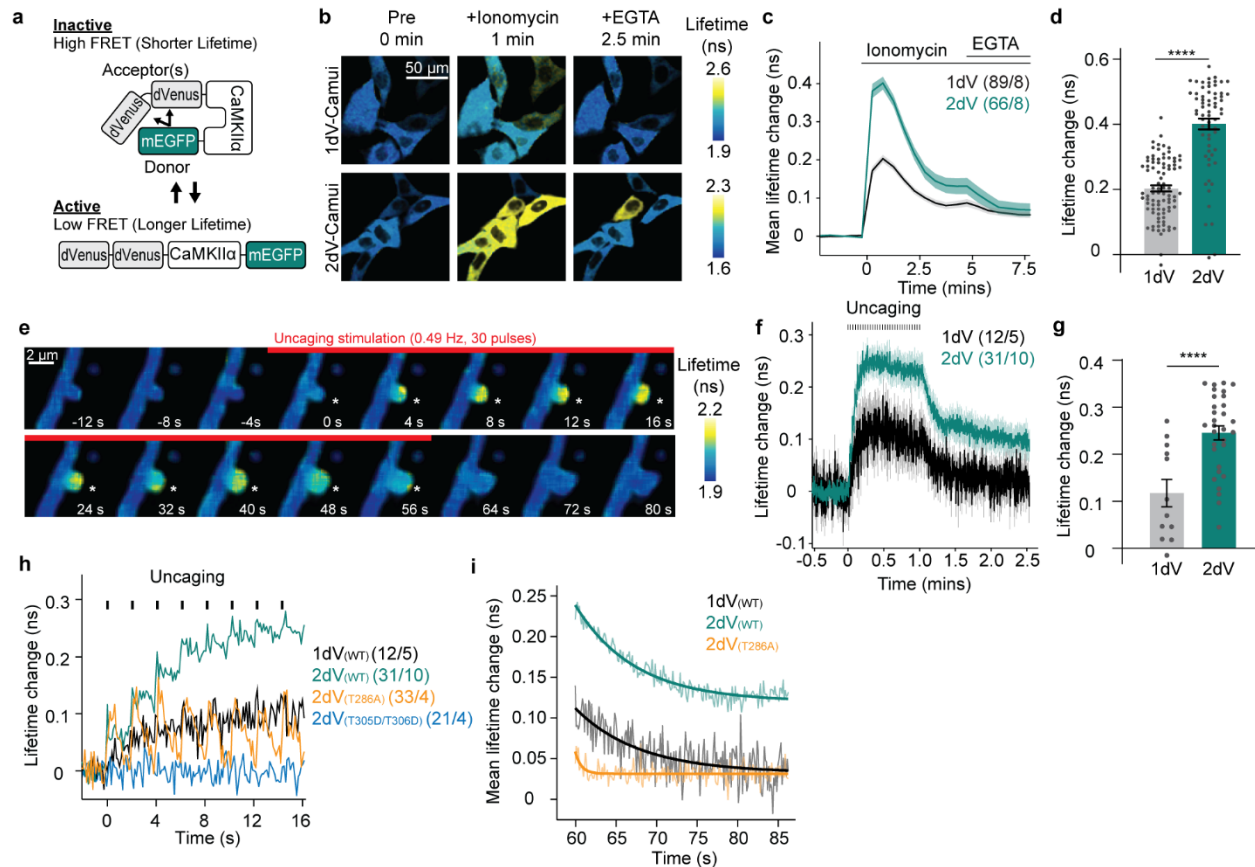
Figure 2: Optimization and characterization of novel conformational CaMKII FRET sensor.

a, A schematic of Camuiα-2dv CaMKII sensor where N- and C-termini of CaMKIIα are labeled with donor EGFP and 2 dimVenus acceptor fluorophores. Activation of CaMKII results in a conformational change and a decrease of FRET efficiency.

b, Fluorescence lifetime images of HeLa cells expressing Camuiα-2dV (top) or original Green Camui with 1 dimVenus (1dV-Camui) (bottom) before, during ionomycin and during EGTA.

c-d, Averaged time course (**c**) and summary of the peak (1 min post drug application) (**d**) of fluorescent lifetime changes of 2dV-Camui (2dV) and Green Camui (1dV) in

response to bath application of ionomycin (3 µM) in HeLa cells. 2dV-Camui showed ~2 fold higher sensitivity. Numbers of samples are in the figure (cells / cultures).

e, Fluorescence lifetime images of CA1 dendrites in hippocampal culture before, during, and after glutamate uncaging at 0.49 Hz in zero extracellular Mg^{2+}.

f-g, Averaged time course (**f**) and summary of the peak (6-11th uncaging pulses) (**g**) of fluorescence lifetime changes in stimulated spines and adjacent dendritic shafts. The numbers of samples are in the figure (spines / cells).

h, Closer view of the lifetime change during first 8 uncaging pulses in 2dV-Camui wildtype (2dV WT), Green-Camui wildtype (1dV WT), 2dV-Camui T286A, and 2dV-Camui T305D/T306D. The numbers of samples are on the figure (spines/cells).

i, The decay kinetics in spines after uncaging. The fitting curve indicate single exponential fitting ($y = A\exp(-t/\tau) + B$, where the fast time constant (τ) is 7.9, 7.3 and 0.74 s for 1dV WT, 2dV WT, and 2dV T286A, respectively.

*** $p < 0.001$, **** $p < 0.001$, Two-tailed t-test.
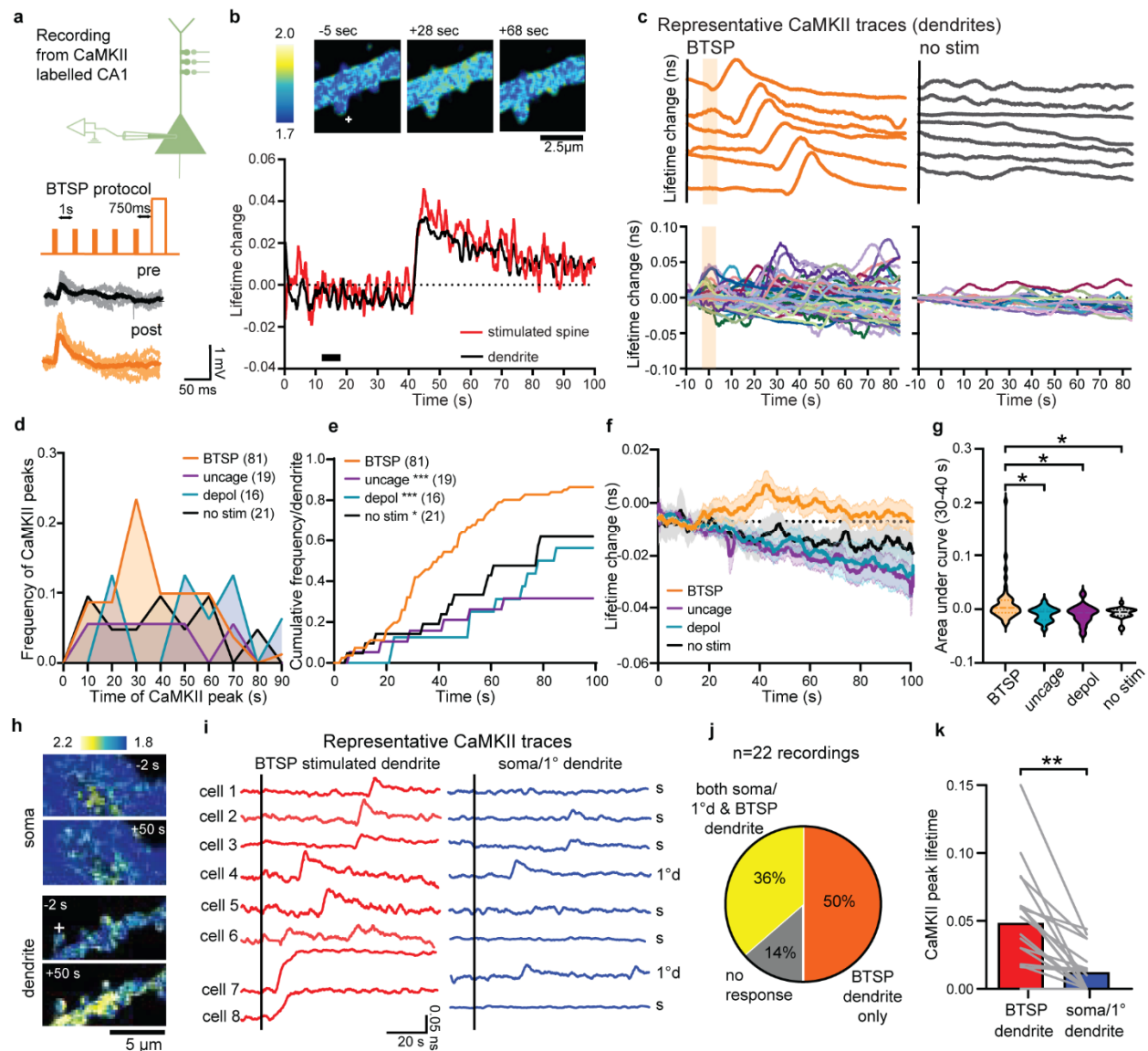
Figure 3. Dendritic, delayed, and stochastic CaMKII activation (DDSC) during BTSP induction.

a, Schematics of the experimental setup (top), BTSP protocol (mid), and raw traces of 10 EPSPs and mean pre and post-BTSP protocol (bottom).

b, A representative fluorescence lifetime images (top) and time course (bottom) of a dendritic segment expressing 2dV-Camui during BTSP induction. "+" depicts the BTSP

stimulated spine. Images are acquired at 128 ms / frame and the time course was filtered with a moving average over 60 frames.

c, Top, 6 representative traces of delayed dendritic CaMKII activity (filtered) measured as fluorescence lifetime changes of 2dV-Camui in dendrites in BTSP and non-stimulated (non-stim). Bottom, Lifetime change plots of all dendritic activity in BTSP (n=81), non-stim (n=21). The shaded bars show the BTSP protocol.

d, Frequency of DDSC onsets after BTSP induction (orange) compared with uncaging only (uncage), current injection only (depol), and no stimulation (no-stim) controls. Numbers of dendrites are in the figure.

e, Cumulative frequency of **d**. $*p < 0.05$, $***p < 0.001$, Kolmogorov-Smirnov test against BTSP.

f-g, Average time course (**f**) and area under the curve (30-40 s post-BTSP) (**g**) of mean lifetime change of CaMKII activity under BTSP, non-stimulated (no-stim), current injection only (depol), and uncaging-only (uncage) conditions. $*p<0.05$, one-way ANOVA followed by multiple comparison tests with Dunnett's correction).

h-k, DDSC does not propagate to the soma or primary dendrites.

h, Representative fluorescence lifetime images of 2dV-Camui lifetime changes before (-10 sec) and after (+50 c) BTSP protocol at the secondary dendrites or the soma.

i, Representative 2dV-Camui traces of the dendrite (red) and the soma (s) or the primary dendrite (1°d) (blue) from 8 different cells. In some samples, soma was not in the same z plane as the stimulated dendrite, and thus primary dendrite was used.

j, Pie chart showing that out of 22 recordings, 50% showed an increase in CaMKII activity, specifically in the dendrites but not in the soma or primary dendrite. 36% of the recordings showed a CaMKII activity increase in both stimulated dendrite and soma/primary dendrite, ad 14% of the dendrites showed no detectable CaMKII activity.

k, The amplitude of DDSC in BTSP-induced dendrites is significantly higher than that in the soma or primary dendrite. ***$p<0.001$, paired t-test.
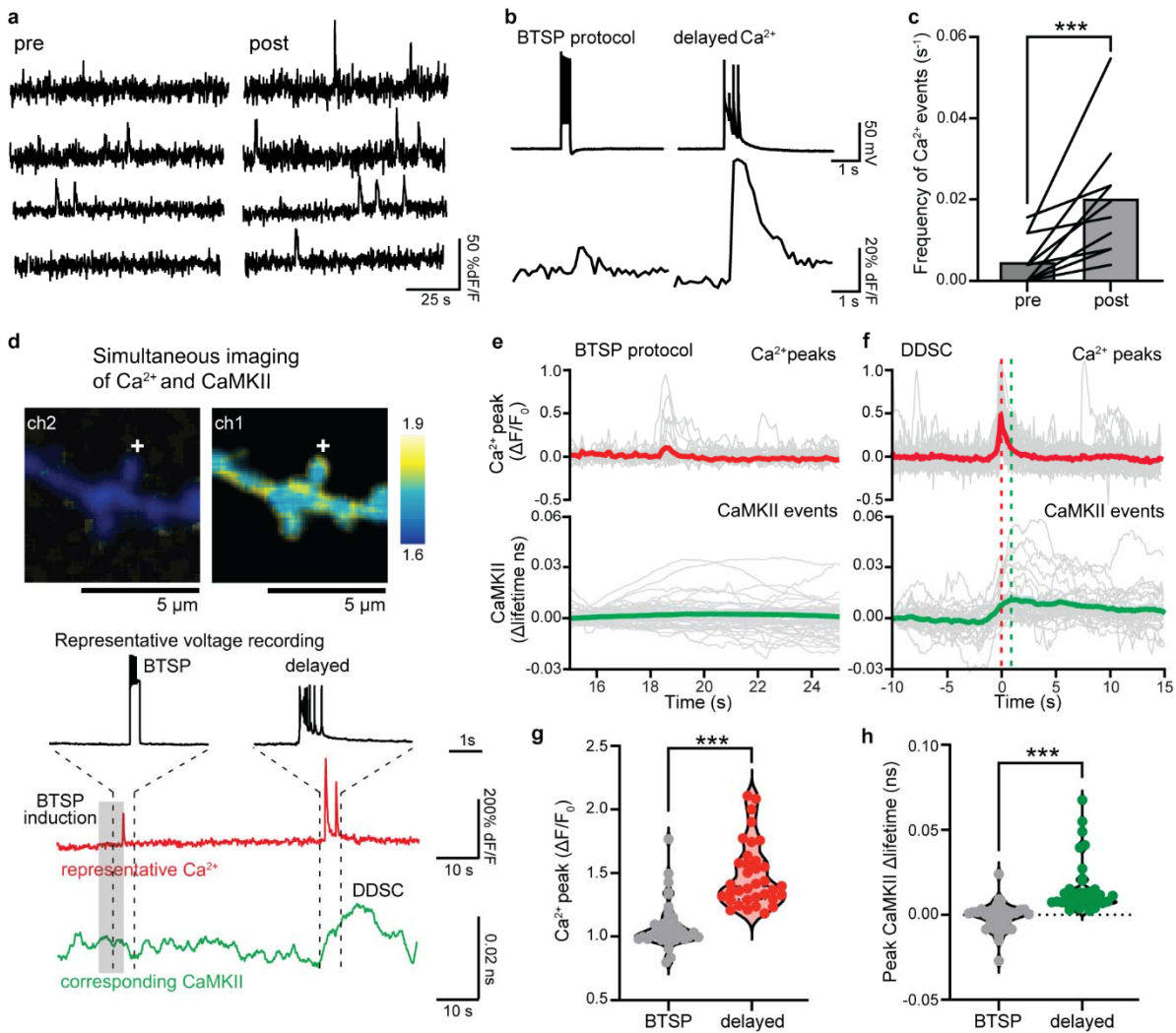
Figure 4: Ca^{2+} imaging shows an increase in Ca^{2+} spikes after BTSP.

a, Snippet of Ca^{2+} traces before (4 min) and after (4 min) BTSP induction in neurons filled with Cal-590 (50 µM) through patch pipette.

b, Representative traces of voltage recordings and corresponding Ca^{2+}.

c, The frequency of Ca^{2+} events before after BTSP induction (n = 12). Paired two-tailed t-test, *p<0.05.

d, Top: Representative fluorescence lifetime images of a dendrite during simultaneous Ca^{2+} (Cal-590) and CaMKII imaging. Bottom: Representative voltage, Ca^{2+} and CaMKII time courses.

e, Average Ca^{2+} elevation (red) and CaMKII activity (green) in the stimulated dendrite during BTSP protocol (n = 37). There was no detectable CaMKII activation during the BTSP protocol.

f, Average of Ca^{2+}-event-triggered average of Ca^{2+} (red) and CaMKII events (green) following BTSP induction (n = 37).

g-h, Summary of Ca^{2+} (**g**) and CaMKII (**h**) peak amplitudes observed during BTSP protocol (as in **e**) and after BTSP induction (as in **f**). ***p < 0.001 two-tailed unpaired test.
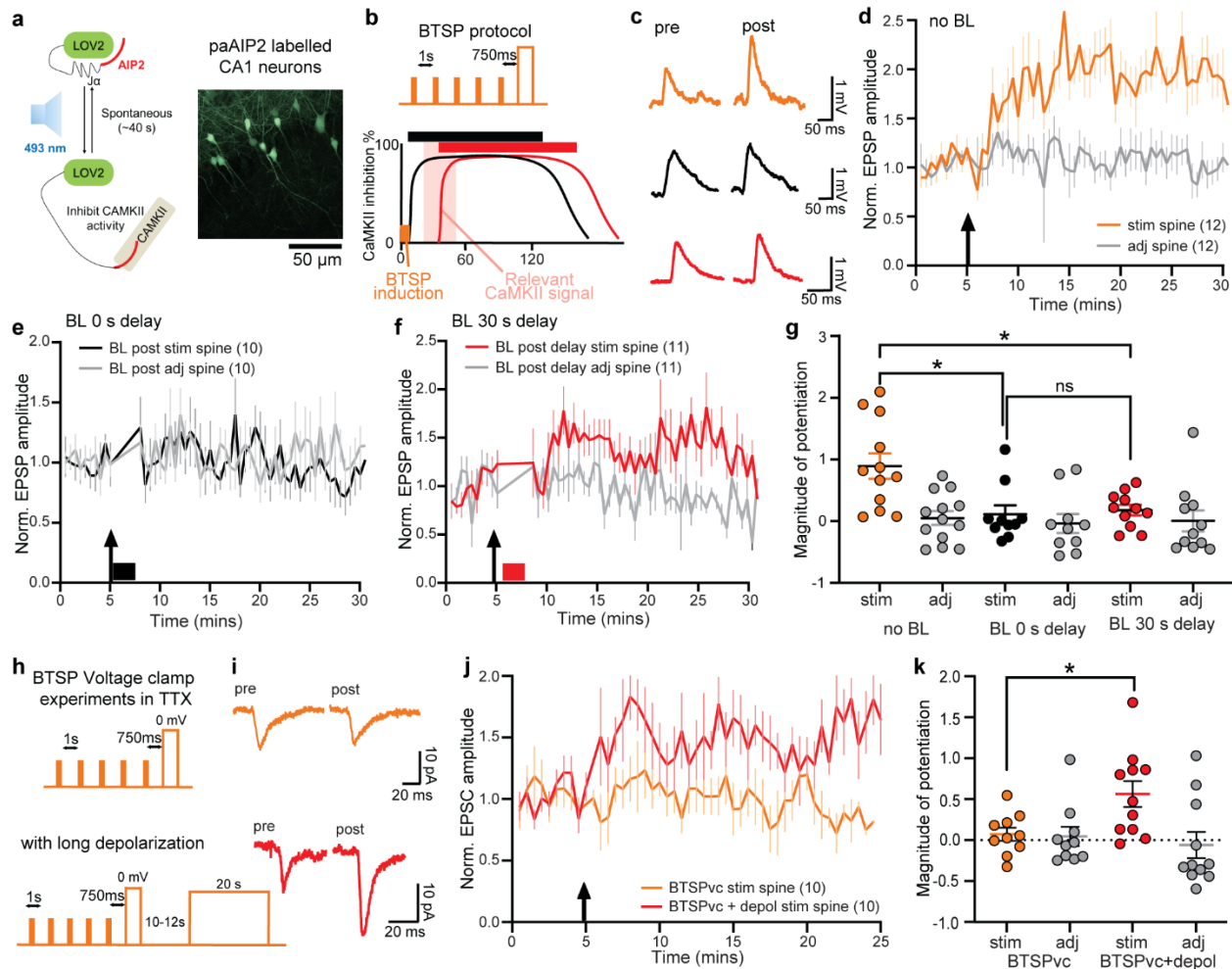
Figure 5: Optical inhibition and voltage clamp experiments show that DDSC plays a critical instructive role in BTSP.

a, Schematics of photoactivatable CaMKII inhibitor paAIP2. Left: Schematics of paAIP2. Upon absorption of blue light (BL, 470 nm), light-oxygen voltage 2 (LOV2) domain changes its conformation, and exposed AIP2 inhibits CaMKII. When the BL is stopped, the paAIP2 becomes inactive within ~40 s. Right: paAIP2-P2A-EGFP labeled CA1 neurons.

b, Schematics of the two separate CaMKII inhibition experiments. CaMKII was inhibited for 2 mins, 0 (black) sec or 30 s (red) after the BTSP protocol (orange).

c, Representative EPSP traces of a stimulated and adjacent spine (average of 10 traces) pre and post BTSP induction in paAIP2 labeled neurons where no BL stimulation was given (orange), or BL with 0 s delay (black) or 30 s delay (red).

d-f, Normalized EPSP time course of EPSPs in response to BTSP in the stimulated spines (n=12) but not in the adjacent spines (n=12) for no BL (**d**), BL with 0 s delay (n=10) (**e**) or BL with 30 s delay (n=11) (**f**). Arrow depicts the timing of BTSP induction (also in e and f).

g, Summary of the magnitude of EPSP potentiation (25-30 min) in stimulated and adjacent spines in no BL, BL 0 s after BTSP protocol (BL 0 s delay), and BL 30 s after BTSP protocol (BL 30 s delay). *p < 0.05, Two-way ANOVA followed by posthoc multiple comparisons with Tukeys' correction.

h, Top: BTSP protocol in voltage clamp (BTSPvc), where a train of 5 uncaging pulses (1 Hz) was paired with depolarization to 0 mV for 300 ms with 750 ms delay after the last pulse under the presence of TTX. Bottom: A protocol to artificially induce delayed CaMKII activity in addition to BTSPvc. We applied additional depolarization ~10-12 s after BTSPvc (BTSPvc+depol).

i, Representative EPSP traces of stimulated spine (average of 10 traces) before (black) and 20 mins after (orange) BTSPvc or BTSPvc+depol.

j, Normalized EPSC amplitude time course in response to BTSPvc protocol (orange) and BTSPvc plus delayed depolarization (red). Arrow is the timing of BTSPvc. Numbers of cells are in the figure.

k, Summary of the magnitude of potentiation of stimulated and adjacent spines during

BTSPvc and BTSPvc+depol (* $p < 0.05$, two-way ANOVA followed by posthoc multiple

comparison's test (Tukey's correction).
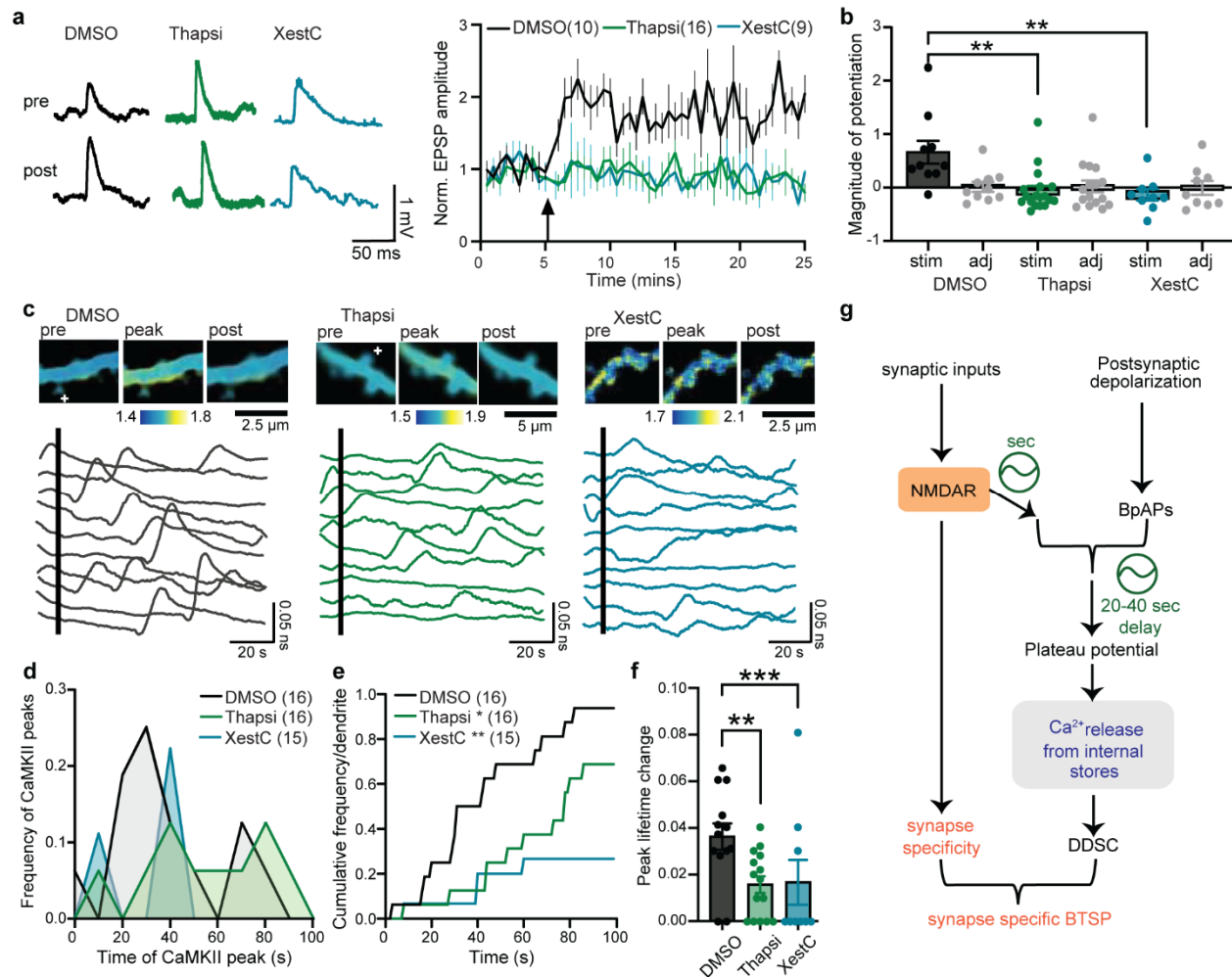
Figure 6: Calcium release from internal stores underlies BTSP and DDSC.

a, BTSP-induced synaptic potentiation is impaired by depleting Ca2+ internal store with thapsigargin (Thapsi, 1 µM) or inhibiting IP3R with Xestospongin-C (XestC, 1 µM) compared with vehicle (DMSO). EPSP traces (left) and averaged synaptic potentiation in the stimulated spines (right) are shown. Numbers of samples are in the figure.

b, Summary of the magnitude of EPSP potentiation for data in (**a**) **p < 0.01, Two-way ANOVA, with multiple comparison test (Tukey's correction).

c, Top: Fluorescence lifetime images of a dendrite showing lifetime change before, during and after a CaMKII peak in DMSO (left), thapsigargin (mid), and XestC (right). Bottom: 10 smoothened dendritic lifetime traces showing DDSC under each condition.

d, The time course of the frequency of DDSC onset under DMSO, thapsigargin, or XestC conditions.

e, Cumulative histogram of (**d**) *p <0.05, ***p<0.001 Kolmogorov-Smirnov test.

f, Summary of peak DDSC amplitude. **p<0.01, ***p<0.001. Two-way ANOVA with multiple comparisons (Tukey's correction).

g, A revised model of BTSP induction. Synaptic inputs activate NMDAR-dependent signaling to prime the stimulated synapses. Combined synaptic inputs and postsynaptic activation lead to delayed plateau potentials. Ca^{2+} signal is further enhanced by intracellular Ca^{2+} release, leading to delayed CaMKII activation (DDSC). DDSC acts as an instructive signal with an extended time window of 20-40 s. Additional signals in spines must provide Synapse specificity (orange).
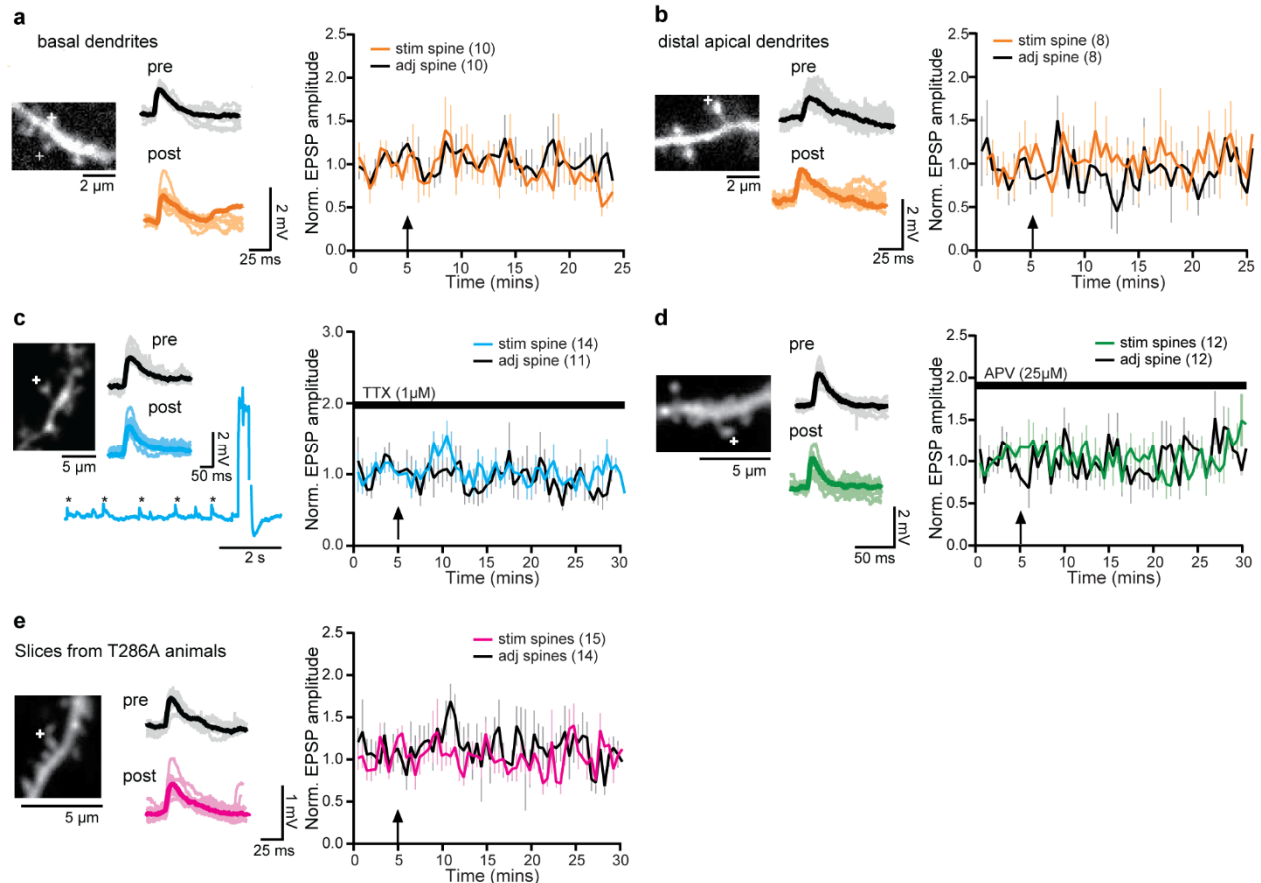
Extended Figure 1: BTSP fail to induce in basal or distal synapses and is dependent on TTX, APV and CaMKII.

a, Right: Representative basal dendritic image where BTSP was induced in one spine (+); Bottom: raw traces of EPSPs in stimulated spine before and after BTSP induction. Left: Averaged time course of normalized EPSP amplitude following BTSP induction in basal dendrites in stimulated and adjacent spines. N is indicated in the figure.

b, Same as (**a**) but in distal dendrites.

c, Right: Representative image of a dendritic shaft, where BTSP protocol was induced in one spine (+) in the presence of TTX (1 µM). All experiments were performed after incubating the slices for ~30 mins in TTX. Bottom: Raw traces of EPSP in the stimulated spine in TTX. 10 EPSPs and mean before (black) and after (blue) BTSP induction. Left: Averaged time course of normalized EPSP amplitude in TTX in stimulated and adjacent spines.

d, Right: Same as (**c**), but performed after incubating the slices for 30 mins in the presence of APV (25 µM).

e, Right: Same as (**c**), but in hippocampal slices made from CAMKIIα[T286A] mice.

1
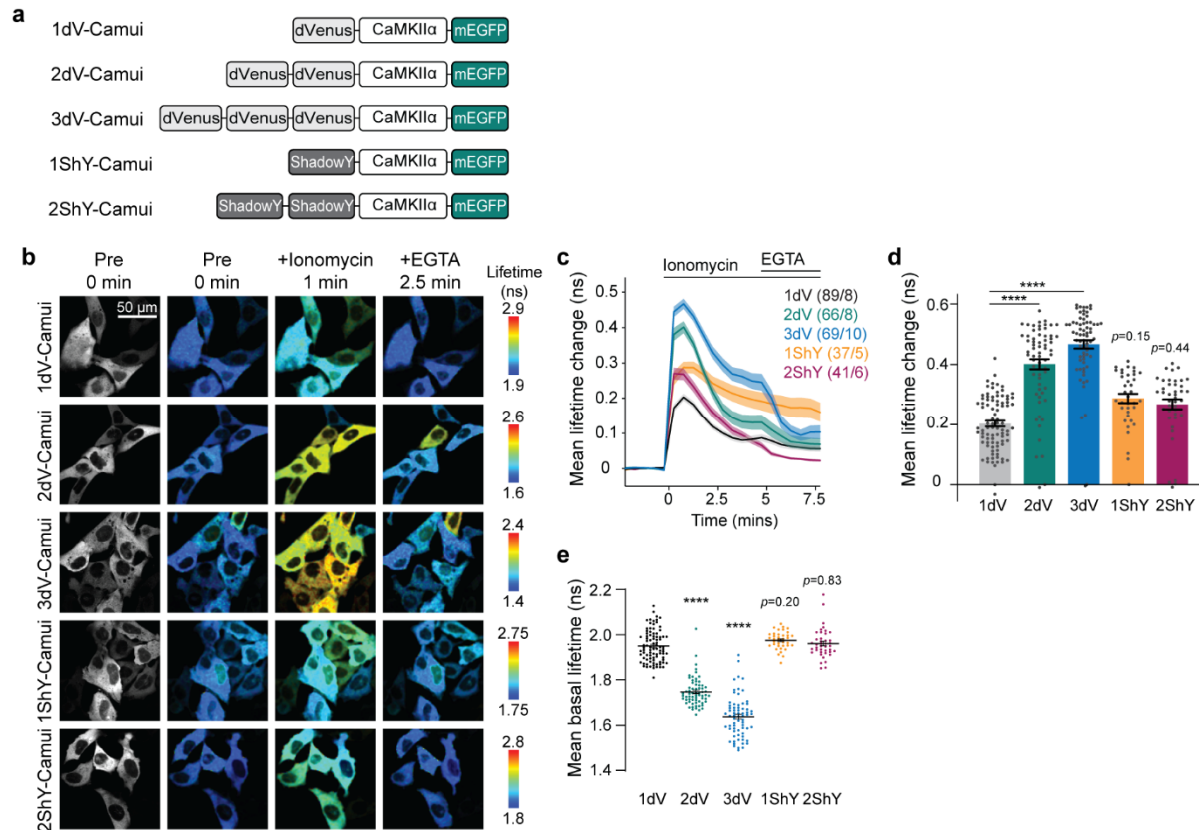
**Extended Figure 2-1: Characterization of novel conformational CaMKII FRET sensor.**

a, A schematic of screened CaMKII sensors where N- and C-termini of CaMKIIα are labeled with 1 to 3 dimVenus or 1 to 2 ShadowY acceptor(s) and donor EGFP fluorophores.

b, Grayscale and fluorescence lifetime images of Hela cells expressing each Camuiα sensor variants. Each image is before (pre), 1 minute after ionomycin (3 μM) and 2.5 minutes after EGTA (8 mM) application.

c-d, Averaged time course (**c**) and summary of the peak (1 min post-ionomycin application) (**d**) of fluorescent lifetime changes of 2dV-Camui (2dV) and Green-Camui (1dV) in response to bath application of ionomycin in HeLa cells. The numbers of each sample are shown in the figure (cells/cultures).

e, Averaged basal lifetime of each CaMKII sensor. Multiplying dimVenus acceptors showed significantly lower basal lifetimes indicating higher FRET efficiency.

The data are presented as mean $\pm$ SEM., **** p < 0.0001, One-way ANOVA followed by Dunnet's post hoc test.

2
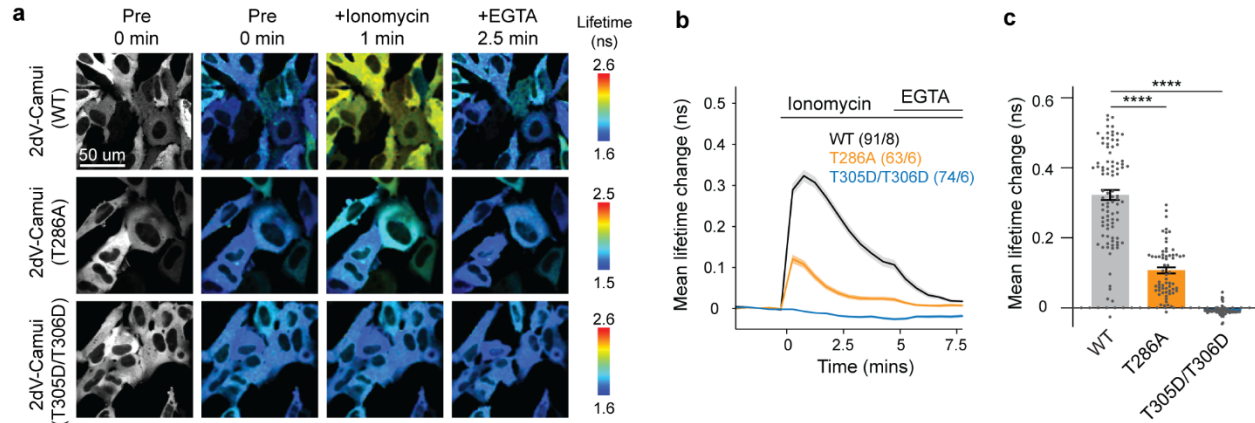
**Extended Figure 2-2: Validation of 2dV-Camui conformational CaMKII FRET sensor with wildtype, T286A or T305D/T306D CaMKII mutants.**

a, Grayscale and fluorescence lifetime images of Hela cells expressing 2dV-Camuiα sensors, which have wildtype CaMKII (WT), CaMKII mutant deficient autonomous activation (T286A), or CaMKII mutant deficient in Ca2+/calmodulin binding (T305/T306D). Each image is before (pre), 1 minute after ionomycin (3 μM) and 2.5 minutes after EGTA (8 mM) application.

b-c, Averaged time course (**b**) and summary of the peak (1 min post-ionomycin application) (**c**) of fluorescent lifetime changes of 2dV-Camui (2dV) and Green-Camui (1dV) in response to bath application of ionomycin in HeLa cells. The numbers of each sample are shown in the figure (cells/cultures).

The data are presented as mean□±□SEM., **** p < 0.0001, One-way ANOVA followed by Dunnet's post hoc test.

3
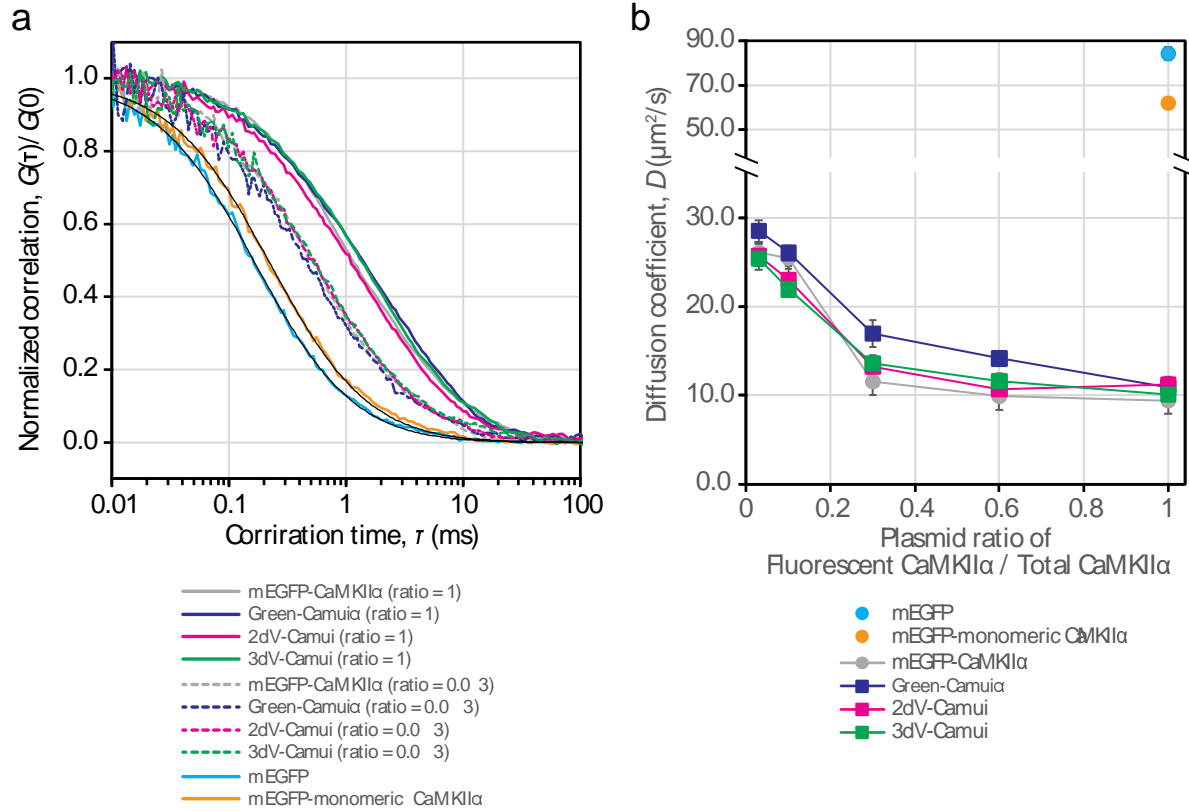
Extended Figure 2-3 Fluctuation correlation spectroscopy (FCS) analysis of CaMKII sensors

a, Normalised correlation curves obtained from 2-photon TCSPC (Time-Correlated Single Photon Counting) FCS for the indicating samples in HEK293FT cell lysate. To investigate whether the sensors were co-polymerised with nonlabelled CaMKIIα, the cells were co-transfected with nonlabelled CaMKIIα at the indicating plasmid ratios. Black lines show fit curves of a correlation function given by:

$$G(\tau) = G(0)\left(1 + \frac{\tau}{\tau_{xy}}\right)^{-1}\left(1 + \left(\frac{w_{xy}}{w_z}\right)^2 \frac{\tau}{\tau_{xy}}\right)^{-\frac{1}{2}}$$

where $G(0)$ is the correlation at time 0, τ is the correlation time, w_{xy} is the lateral and w_z the axial $1/e^2$-radii of the 2-photon excitation volume, which were measured as 0.34 μm and 1.49 μm, respectively, by scanning 0.1-μm fluorescent bead. The diffusion coefficient $D = w_{xy}^2/8\tau_{xy}$ was determined from the average lateral diffusion time τ_{xy} obtained by curve fitting.

b, Diffusion constants of the sensors or mEGFP-CaMKIIα co-expressed with non-labelled CaMKIIα at various plasmid ratios. The diffusion coefficients (ratio = 1) were 9.4 ± 1.5 μm^2/s for mEGFP-CaMKIIα, 11 ± 0.6 μm^2/s for Green-Camuiα, 11 ± 0.9 μm^2/s for 2dV-Camui, 10 ± 0.9 μm^2/s for 3dV-Camui, 84 μm^2/s for EGFP, and 63 μm^2/s for monomeric CaMKIIα (truncated CaMKIIα [1-306]), respectively. Error bars denote SD.

4
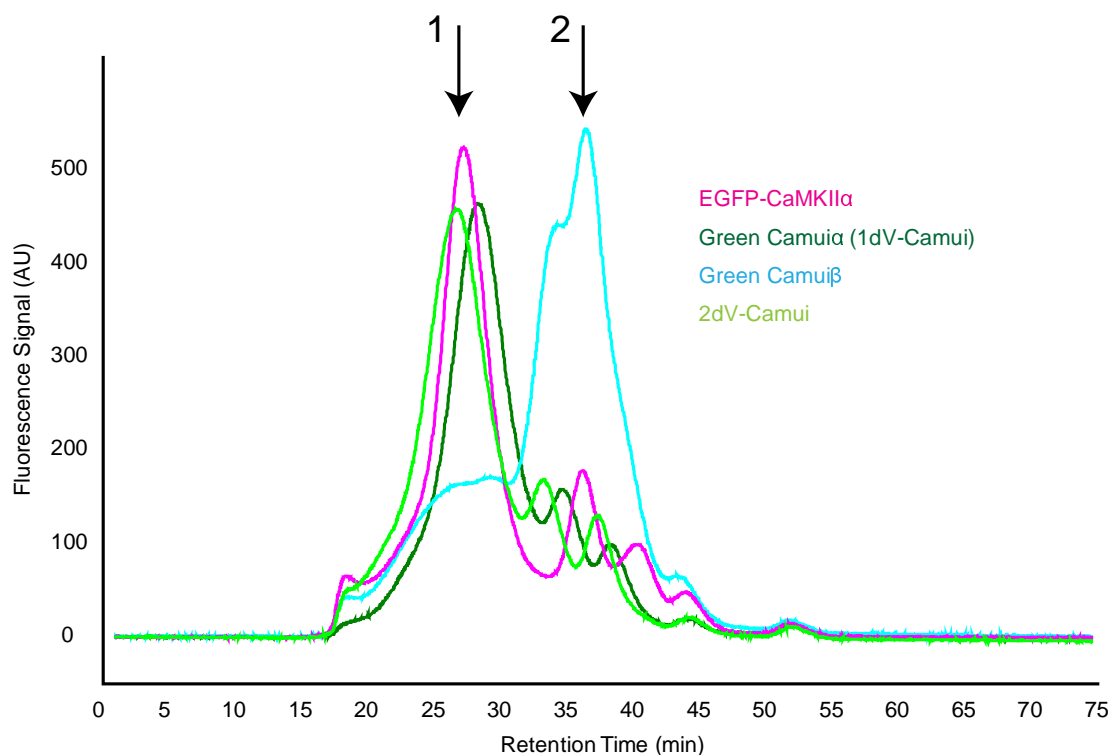
Extended Figure 2-4 Chromatography assay of CaMKII sensors

To estimate the approximate oligomeric state of CaMKII sensors, we performed FSEC on EGFP-CaMKIIα and various Camui proteins expressed in HEK293 cells by transient transfection. The cell lysates expressing these proteins were directly injected to a Superose-6 column, and EGFP fluorescence was detected using 475/507 nm excitation/emission wavelengths. Green Camuiα (1dV-Camui), Green Camuiβ, in which CaMKIIβ subunit is used instead of CaMKIIα, and 2dV-Camui. 2dV-Camui-2dV showed a similar retention time to EGFP-CaMKIIα and 1dV-Camui (peak at ~27 min; arrow 1), suggesting formation of a dodecamer. However, Green Camuiβ showed a high fraction of lower oligomeric species represented by a peak at ~35 min (arrow 2).

5
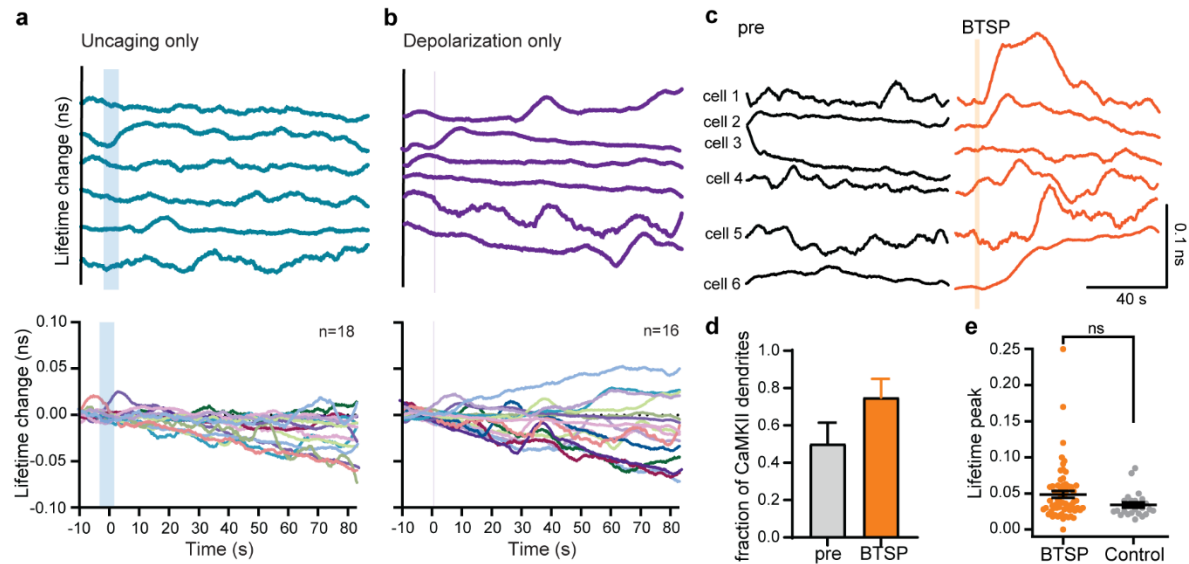
Extended Figure 3-1: **Control experiments show that delayed dendritic CaMKII is specific to BTSP induction.**

a-b, Top, Representative traces of CAMKII dendritic activity (smoothened by moving average of 60 points, 7.8 frames per seconds) of uncaging only and depolarization only experiments. Bottom, Lifetime change of all dendritic CaMKII activity for uncaging only (n=16) and depolarization only (n=19). The shaded region in representative and summary plots show where uncaging or depolarization was provided.

c, Representative traces of smoothened Camuiα-2dv dendritic recording before (black) and after (orange) the BTSP protocol.

d, Fraction of dendrites showing CaMKII activity in pre versus after induction of BTSP condition.

e, Peak amplitude of CaMKII activation in responsive BTSP dendrites versus control dendrites (combined no-stim, uncaging only, and depolarization only) (p = 0.078, unpaired two-tailed t-test).
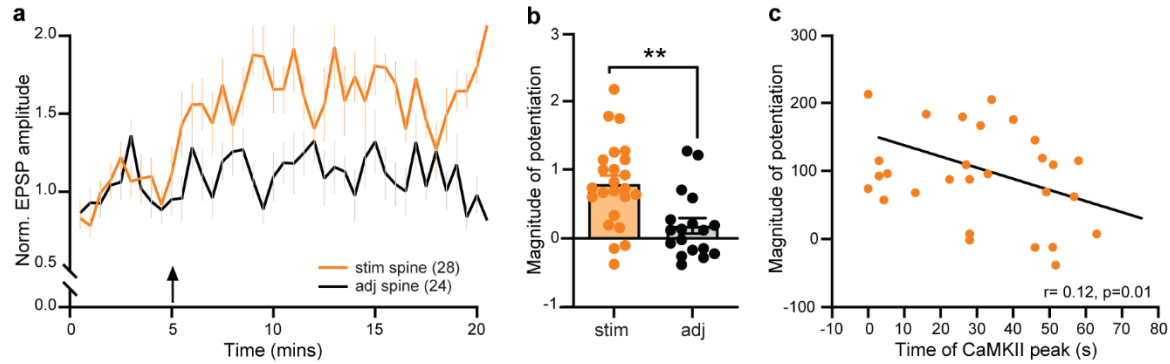
Extended Figure 3-2: BTSP-induced synaptic potentiation is induced in 2dV-Camui labeled neurons.

a-b, Averaged time course (**a**) and summary (25-30 min, **b**) of normalized EPSP amplitude in neurons expressing 2dV-Camui in the stimulated and adjacent spines. **p < 0.01, unpaired two-tailed t-test.

c, Correlation between the magnitude of potentiation and the time of CaMKII peak after the BTSP protocol. The graph shows an inverse correlation such that earlier CaMKII activity results in a higher magnitude of potentiation (n=28 pairs, r^2 = -0.12, p < 0.01).
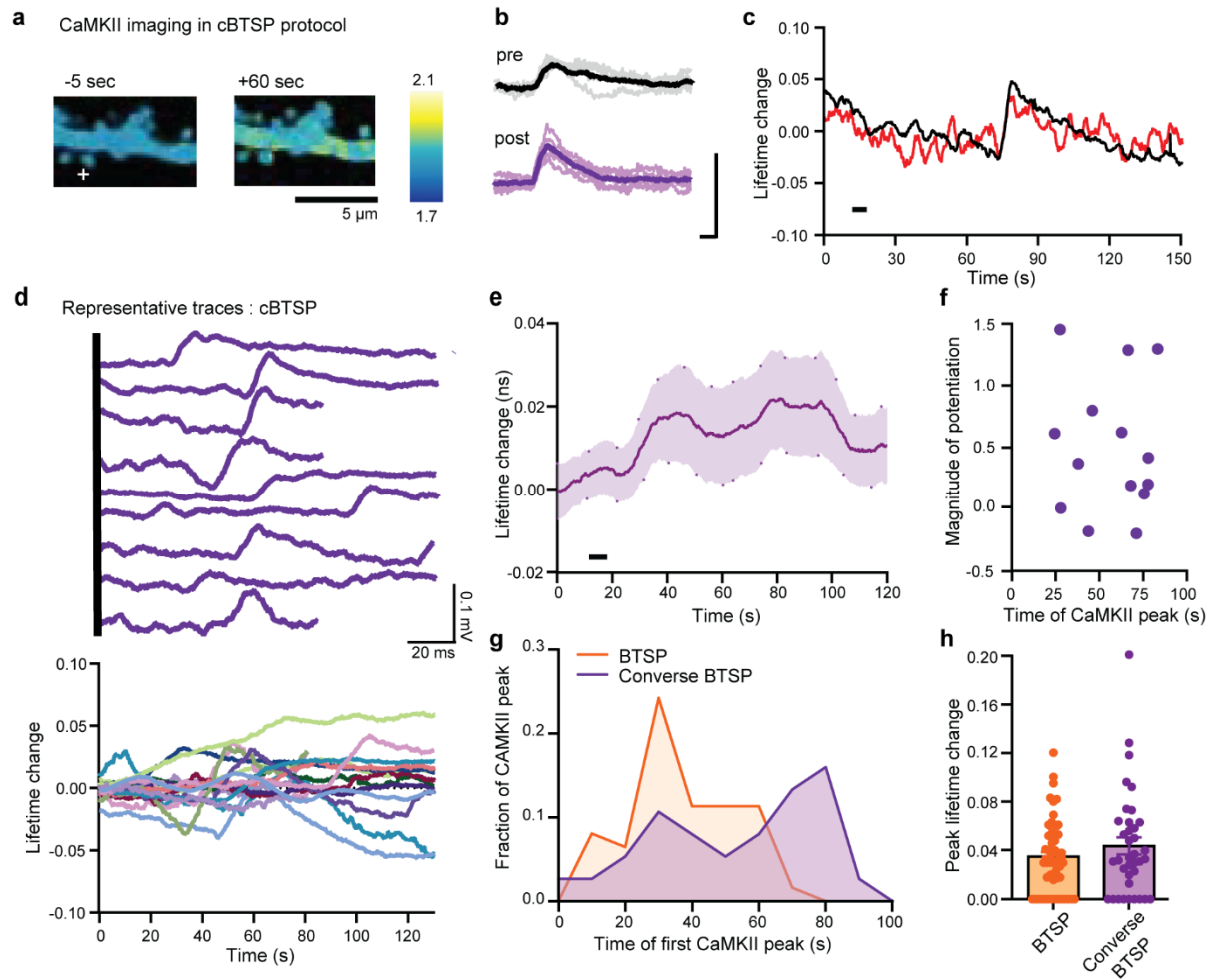
Extended Figure 3-3: Converse BTSP protocol induces delayed dendritic and stochastic CaMKII (DDSC).

a, Fluorescence lifetime images a 2dV-Camui expressing dendrite before, during and after the converse BTSP (cBTSP) protocol.

b, Representative EPSP traces from stimulated spines before and after the cBTSP protocol. 10 traces and mean for each.

c, Time courses of fluorescence lifetime changes in the stimulated spine and nearby dendrite from the dendrite in (**b**) (filtered). Black bar, cBTSP protocol.

d, Top: Representative dendritic 2dV-Camui recordings. Bottom: All 2dV-Camui recordings (filtered) during uCBTSP induction.

e, Mean + SEM lifetime change of dendritic 2dV-Camui recordings in response to cBTSP induction.

f, Relationship between the magnitude of potentiation and the time of the first CaMKII peak after cBTSP protocol (n=15 pairs, r^2=0.02, p=0.6).

g, The frequency of CaMKII events (onset) as a function of time from the cBTSP protocol.

**h,** Peak amplitude of CaMKII activation events before and after the cBTSP protocol.

9
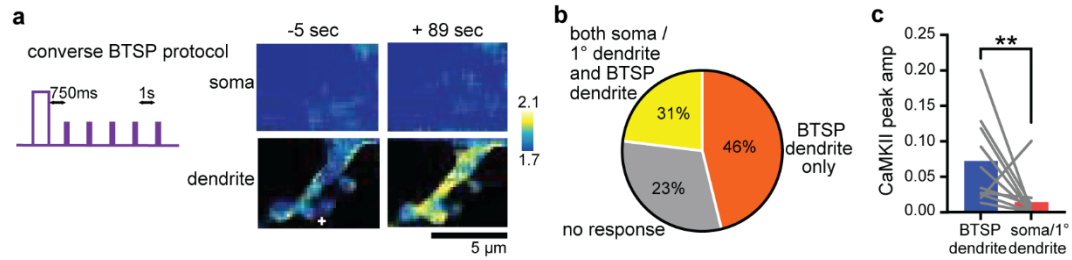
Extended Figure 3-4: DDSC induced by converse BTSP protocol does not spread to the soma.

a, Simultaneous FLIM imaging of 2dV-Camuiα in soma and stimulated dendrite during cBTSP.

b, Pie chart for 14 recordings, out of which 46% showed an increase in CaMKII activity specifically in the dendrites but not in soma or primary dendrite. 31% of the recordings showed an increase in CaMKII activity in both the stimulated dendrite and the soma/primary dendrite and 23% of the dendrites showed no CaMKII activity.

c, Peak amplitude of CaMKII activation events in the stimulated dendrite compared with that in the soma or the primary dendrite. **p<0.01. Paired two-tailed t-test.
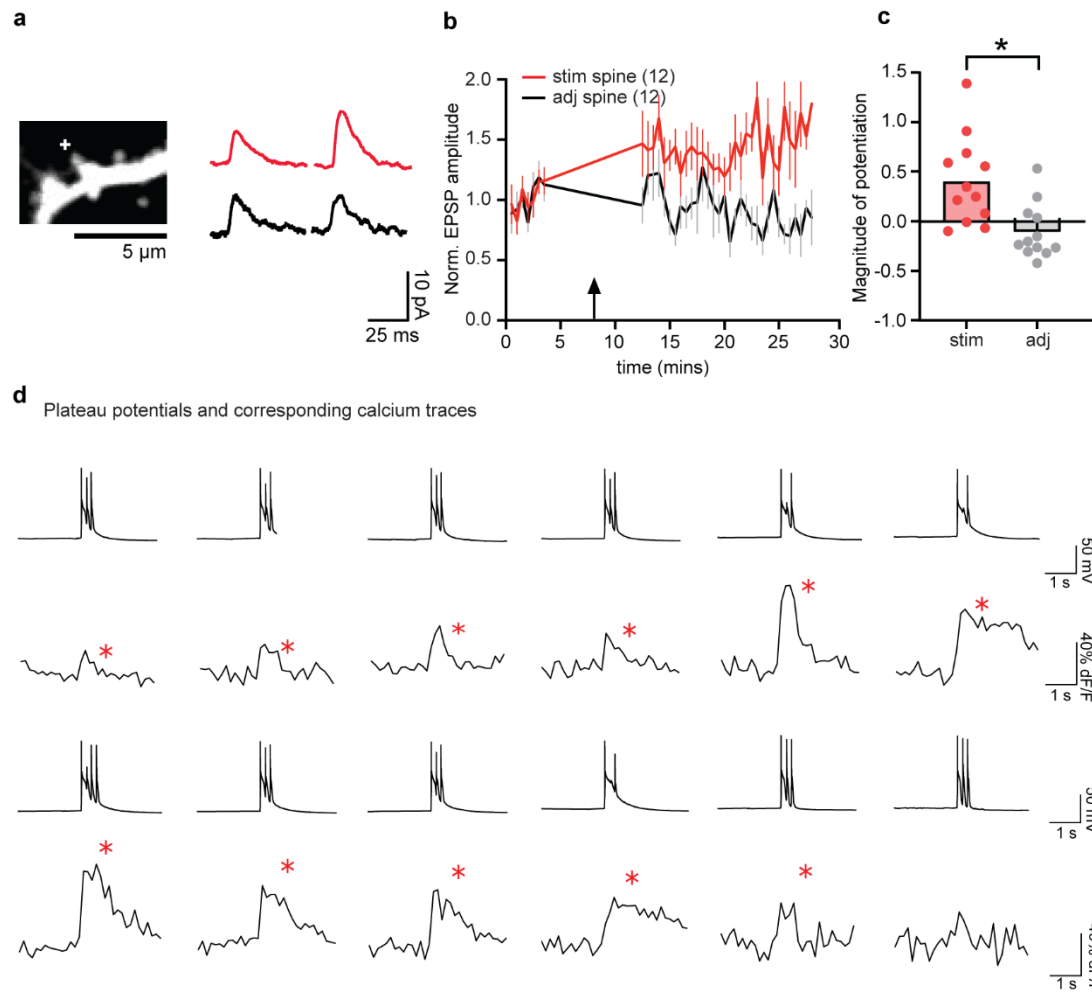
Extended Figure 4-1: BTSP induces EPSP potentiation and plateau potentials observed during Ca^{2+} imaging experiments.

a, A representative dendrite of a neuron loaded with Cal-590. Left: dendrite image, Right: EPSP traces before and after BTSP protocol.

b, Averaged time course of normalized EPSP amplitude in stimulated and control spines. The gap in EPSP recording shows the time of calcium imaging (**Fig. 4a-c**).

c, Group summary plot shows a higher magnitude of potentiation in stimulated spines (n=12) than adjacent spines (n=12, *p < 0.05, two-tailed t-test).

d, Representative traces of voltage recordings showing that plateau potentials had corresponding Ca^{2+} traces (red *) in a majority of the examples (58/74, 3-standard deviation for Ca^{2+}).

11
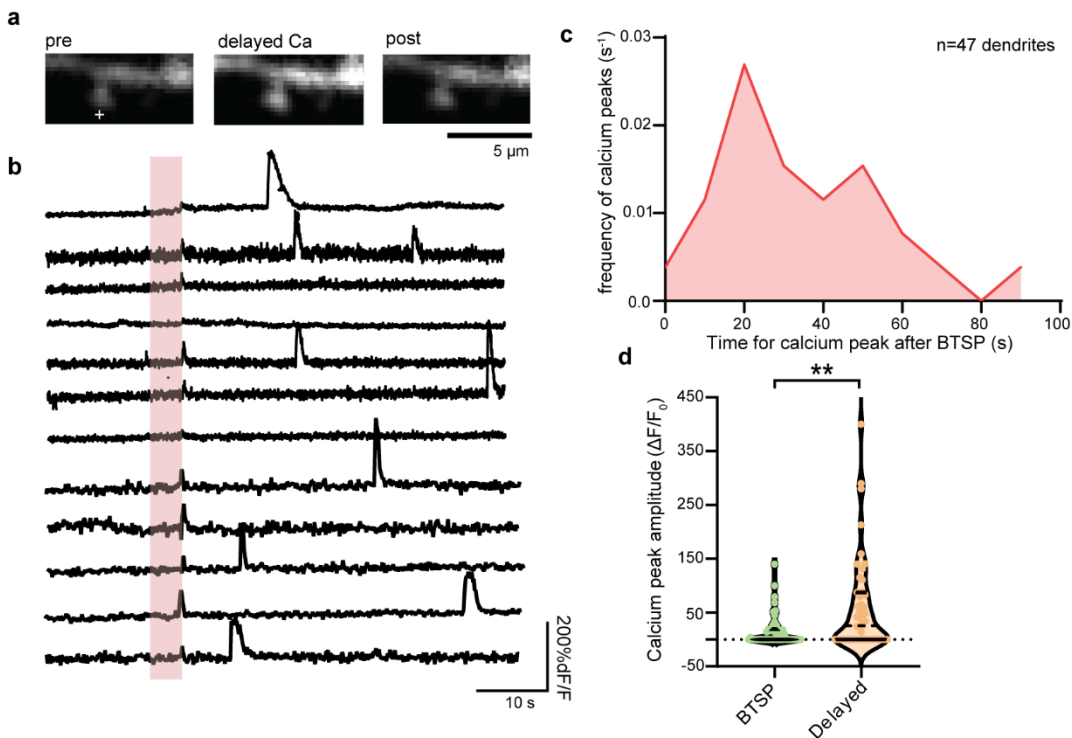
Extended Figure 4-2: Characterization of delayed Ca²⁺ events in response to the BTSP protocol.

a, Representative dendritic shaft filled with Cal 590 dye during a Ca^{2+} event.

b, Representative dendritic calcium traces after the BTSP protocol (pink shadel. The traces show multiple calcium events after BTSP, in addition to smaller event during current injection of BTSP protocol.

c, The frequency of Ca^{2+} events as a function of the time after the BTSP protocol. the frequency peak appears around ~20-30 secs after the BTSP protocol.

d, Ca^{2+} peak amplitude showed a smaller calcium during depolarization and a significantly larger delayed calcium peak amplitude, paired t-test, p<0.01.